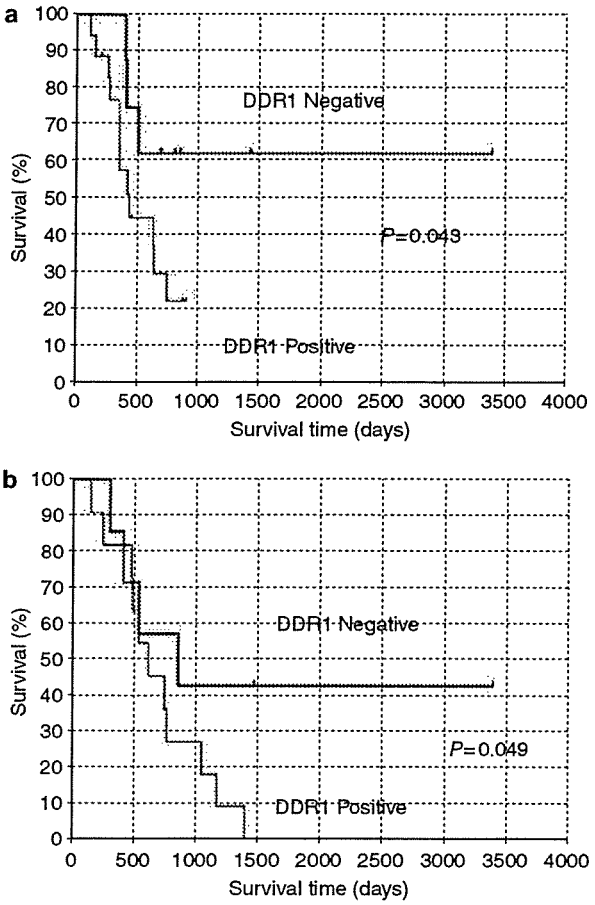

Figure 1 DDR1 protein expressions and patient survivals. Kaplan–Meier survival curves for patients, stratified according to levels of DDR1 expressions in tumors (low DDR1 staining: 0–1 score; high DDR1 staining: 2–3 score; log-rank test). (a) A significant trend for worse outcome was observed in the DDR1-positive group ($P=0.043$). (b) DDR1 protein expressions and patient survivals in independent groups of gliomas. Kaplan–Meier survival curves for patients, stratified according to levels of DDR1 expressions in tumors (low DDR1 staining: 0–1 score; high DDR1 staining: 2–3 score; log-rank test). A significant trend for worse outcome was observed in the DDR1-positive group ($P=0.049$).

groups: positive and negative groups according to immunostaining score. Positive staining for DDR1 was confirmed to be associated with unfavorable overall survival time ($P=0.043$; Figure 1a). Next, in new independent 19 glioma samples, similar results were obtained ($P=0.049$; Figure 1b). Although our results were based on relatively small sample size, the correlation between DDR expression and survival was confirmed by real-time quantitative PCR and also confirmed immunohistochemical analysis in independent samples.

Glioma cell proliferation and invasion are inhibited by DDR1 siRNA

DDR1 overexpression was linked to aggressiveness of glioma in our analysis. In order to determine whether downregulation of endogenous DDR1 suppresses proliferation and invasive behavior of gliomas, we synthesized short interfering RNA (siRNAs) against DDR1 mRNA to reduce expression of DDR1 protein. We analysed efficacy of siRNA-mediated inhibition of DDR1 mRNA synthesis in U251, GI-1, and T98G cells by real-time PCR. As shown in Figure 2a, when U251 cells were transfected with siRNAs against DDR-1 (DDR1-#1 and DDR1-#2), DDR1 mRNA was downregulated 48 h later ($P<0.01$), whereas transfection with a related control siRNA failed to modify DDR1 mRNA expression. When GI-1 and T98G cells were transfected with siRNAs against DDR-1 (DDR1-#1 and DDR1-#2), DDR1 mRNA was downregulated by 10–15% of control siRNA ($P<0.01$).

After transfection with siRNAs against DDR-1, U251 cell counts within 48 h were approximately 40–60% of untreated or control-siRNA-treated cells during this same period of time ($P<0.01$; Figure 2b). GI-1 and T98G cell counts within 48 h were approximately 35–50% of untreated or control-siRNA-treated cells during this same period of time ($P<0.01$). Cell proliferation was significantly suppressed by siRNA against DDR1, as reflected in reduction of mRNA expression.

For invasion assays, transfectants were seeded onto Matrigel-coated invasion chambers, incubated for 24 h and total numbers of cells on the underside of each filter were determined. As shown in Figure 2c, transfections of U251 cells with anti-DDR1 siRNA inhibited cell invasion through the Matrigel by more than 80%, whereas the use of control siRNA had no effect ($P<0.01$). Transfections of GI-1 and T98G cells with anti-DDR1 siRNA inhibited cell invasion through the Matrigel by more than 70–80%, whereas the use of control siRNA had no effect ($P<0.01$). Therefore, invasion by cells was significantly suppressed by siRNA against DDR1, as reflected by reduced mRNA expression.

Discussion

Several works (Sallinen *et al*., 2000; Khan *et al*., 2001; Ramaswamy *et al*., 2001; Rickman *et al*., 2001; Agrawal *et al*., 2002; Kim *et al*., 2002; Veer *et al*., 2002; Vijver *et al*., 2002; Boom *et al*., 2003; Godard *et al*., 2003; Hunter *et al*., 2003; Mischel *et al*., 2003; Nutt *et al*., 2003; Shai *et al*., 2003; Sorlie *et al*., 2003; Freije *et al*., 2004; Mischel *et al*., 2004; Hoelzinger *et al*., 2005; Liang *et al*., 2005; Nigro *et al*., 2005; Rich *et al*., 2005; Somasundaram *et al*, 2005; Wong *et al*., 2005) showed the usefulness of utilizing methods of analysis of multiple forms of data including both clinical and multiple genes, to achieve a more precise discrimination of outcomes for individual patients. The same logical use of multiple forms of data and methods of analysis has been applied in the present study to accurately achieve better classification and prediction of glioma patients. In the present study, we used expression arrays to identify genes that reflect patient's survival. The groups of patients used represented the two extremes of

glioma with respect to outcomes. Nutt *et al.* (2003) and Freije *et al.* (2004) reported the use of microarrays to predict outcomes for glioma patient. Nutt *et al.* involved a group of 50 glioma patients who were not selected based on survival duration. The investigators used Affymetrix U 95 GeneChips to develop a model to classify cases into unfavorable and favorable groups that exhibited significantly different survivals. They picked up 20 genes different from our study that highly correlated with class distinction. On the other hand, Freije *et al.* (2004) also reported the use of microarrays to predict outcomes for all histological types of 85 gliomas. The investigators used Affymetrix HG 133 GeneChips to develop a 44-gene model to classify cases into unfavorable and favorable groups that exhibited significantly different survivals. From these two studies, there were no attempt to predict survivals of individual patients, but results were consistent with ours, and together suggested that clinical differences in outcomes were reflected in global patterns of gene expression that could be appreciated using microarrays.

Some of the genes that were critical components of patterns that were used to discriminate between long-term and short-term survivors are known to affect virulence of the malignant phenotype. Several groups have confirmed prognostic markers of glioma such as Insulin-like growth factor-binding protein 2 (IGFBP2) (Kim *et al.*, 2002; Godard *et al.*, 2003), vascular endothelial growrh factor (VEGF) (Godard *et al.*, 2003), Osteonectin, Doublecortex, Semaphorin 3B (Rich *et al.*, 2005) and brain-type fatty acid-binding protein (FABP7) (Liang *et al.*, 2005).

We have selected *DDR1*, *KSP37* and *DYRK3* from a 21-gene model (21 genes derived from multivariate analysis) to classify cases into unfavorable and favorable groups that exhibited significantly different survivals. We observed that glioma cell proliferation and invasion were significantly suppressed by siRNA against DDR1. The DDR1 is a tyrosine receptor kinase activated by various types of collagen, and is involved in cell–matrix communication (Vogel, 1999). DDR1 is activated independently of β1 integrin (Vogel *et al.*, 2000). DDR1–collagen interaction facilitates the adhesion, migration, differentiation/maturation and cytokine/chemokine production of leukocytes (Yoshimura *et al.*, 2005). DDR1 is overexpressed in several tumors including high-grade brain, esophageal and breast cancers (Weiner and Zagzag, 2000). Based on our data and Ram *et al.* (2005), DDR1 may play a potential role in proliferation and invasion of gliomas. Invasive phenotype is caused by activation of matrix metalloproteinase-2 in DDR1-overexpressing cells (Ram *et al.*, 2006). Glioma cell adhesion, including intercellular and

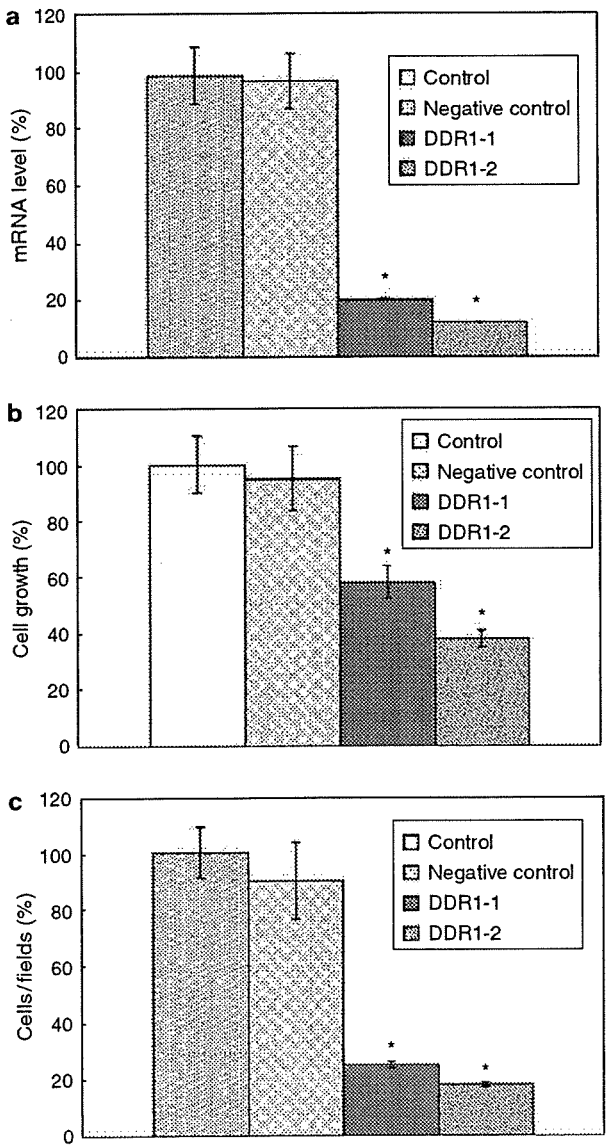

Figure 2 Effects of DDR1 knockdown by RNA interference on proliferation and invasiveness of human glioma cell lines. U251 cells were transiently transfected with short interfering RNAs (siRNA) and subjected to semiquantitative PCR analysis, proliferation assay or Matrigel invasion assays. (a) Reduction of DDR1 mRNA expression by siRNAs against DDR1 was determined by semiquantitative PCR analysis. Transfection with DDR1 siRNAs significantly reduced DDR1, whereas transfection with siRNAs targeted to an unrelated mRNA had no effect on DDR1 expression. $^*P<0.01$ compared with both control groups. (b) Cell proliferation assay. Cells were cultured in 96-well plates in 100 μl of serum-enriched medium. When 80% confluence was reached, 25 μl of 100 nM siRNA in cytofectin was added drop wise. Numbers of viable cells were evaluated after 48 h culture by incubation with Tetra color one, and numbers obtained were compared with those of controls. After transfection with DDR1 siRNAs, U251 cell counts within 48 h were approximately 40–60% of untreated or control-siRNA-treated cells during this same period of time. $^*P<0.01$ compared with both control groups. (c) For the invasion assays, transfectants were seeded onto Matrigel-coated invasion chambers and incubated for 24 h. Total numbers of cells on the underside of each filter were determined. Invading cells were significantly suppressed by siRNAs against DDR1, as reflected by reduction of mRNA expression. Control, no siRNA treatment; negative control, control siRNA treated. DDR1-#1, DDR1-#2; DDR1 siRNA treated. $^{**}P<0.01$ compared with both control groups.

cell–matrix adhesions, is critical to the maintenance of structural integrity, polarity and cell–cell communication, and their expression is frequently observed in tumor cells concordant with a breakdown of cellular organization, causing an uncontrolled leakage of nutrients and other factors necessary for the survival and growth of tumor cells, and loss of cell–cell contact inhibition leading to increased cell motility. Thus, DDR1 may be a novel molecular target for therapy, and provide an important predictive marker for survival in patients with glioma. KSP37 protein is constitutively secreted by Th1-type CD4-positive lymphocytes and lymphocytes with cytotoxic potential, and may be involved in an essential process of cytotoxic lymphocyte-mediated immunity (Ogawa *et al.*, 2001). Down-regulation of KSP37 protein may correlate with poor prognosis of glioma patients with immunosuppressive state. DYRK3 is a member of dual-specificity tyrosine-regulated kinases with roles in cell growth and development. DYRK3 was reported to be expressed in erythroid progenitor cells, and to play roles in kinase activation (Li *et al.*, 2002). Although KSP37 and DYRK3 are unique molecules, their roles in glioma progression are unclear, and should be further investigated in the future.

Regardless of their roles in tumorigenesis, all these markers offer potential clinical applications for the treatment and detection of malignant gliomas. To our knowledge, this study is the first to address these molecules as molecular targets for therapeutics. Values of gene-expression-based predictors for prognosis of malignant glioma patients will not be fully realized until additional therapies are available for patients destined to have poor survival, following conventional chemotherapy. In this regard, expression profiles may not only predict the likelihood of long-term survival following nitrosourea chemotherapy, but may also yield clues on individual genes involved in tumor development, progression and response to therapy. It is likely that some of the most differentially expressed genes such as those discussed above will represent therapeutic molecular targets. Moreover, the ability to histologically distinguish ambiguous gliomas will enable appropriate therapies to be tailored to specific tumor subtypes. Class prediction models based on defined molecular profiles allow classification of malignant gliomas in a manner that will better correlate with clinical outcomes than with standard pathology.

Materials and methods

Patients

Mean age of patients was 53.2 years old (range, 18–80). Twenty-two patients were men and seven were women. Tissues were snap-frozen in liquid nitrogen within 5 min of harvesting, and stored thereafter at −80°C. Clinical stage was estimated from accompanying surgical pathology and clinical reports. Samples were specifically re-reviewed by a board-certified pathologist in our institution, using observation of sections of paraffin-embedded tissues that were adjacent or in close proximity to the frozen sample from which the RNA was extracted. Histopathology of each collected specimen was reviewed to confirm adequacy of the sample (i.e., minimal contamination with non-neoplastic elements), and to assess the extent of tumoral necrosis and cellularity. Histological characteristics of tumor samples and clinical disease stage were included as supplements in Table 1.

After surgical resection of tumor, patients had a course of external beam radiation therapy (standard dose of 40 Gy to the tumor with a 3-cm margin, and 20 Gy boost to the whole brain) and nitrosourea-based chemotherapy. Patients were monitored for recurrences of tumor during the initial and maintenance therapy by magnetic resonance imaging or computed tomography. Treatments were carried out at the Department of Neurosurgery, Niigata University Hospital. Informed consent was obtained from all patients for the use of samples in accordance with the guidelines of the Ethical Committee on Human Research, Niigata University Medical School. Overall survival was measured from the date of diagnosis. Survival end points corresponded to dates of death or last follow-up.

RNA extraction

Total RNA was extracted with 1 ml Isogen (Nippongene, Toyama, Japan) per 100 mg frozen glioma tissues, following the manufacturer's instructions. Each tissue type was homogenized with a Polytron (Fisher Scientific) for 30 s and cleared by a 10-min centrifugation at 10 000 *g*. For each ml Isogen, 0.2 ml chloroform was added and samples were vigorously shaken for 20 s and then incubated on ice for 10 min. The aqueous phase was separated by centrifugation at 10 000 *g* for 10 min, decanted and an equal volume of isopropanol was added. The mixture was allowed to precipitate for 10 min and the precipitate was collected by centrifugation at 12 000 *g* for 10 min. The pellet was washed with 70% ethanol, collected by brief centrifugation, air dried and re-suspended in H_2O. RNA was further purified using an RNeasy column (Qiagen, Valencia, CA, USA). The purified RNA was quantified using a UV spectrophotometer, and RNA quality was evaluated by capillary electrophoresis on an Agilent 2100 Bioanalyzer (Agilent Technologies). Only samples with 28S/18S ratios >0.7 and with no evidence of ribosomal peak degradation were included in the study.

Agilent cDNA microarrays

Agilent human 1 cDNA microarrays (Agilent Technologies) contained 13 156 clones from Incyte's human cDNA library. Test and normal brain RNAs were labeled with both Cy3-dCTP and Cy5-dCTP nucleotides (Amersham Biosciences, Tokyo, Japan) and hybridized on two slides (dye-swap hybridizations) according to the direct-labeling method provided by the manufacturer. Following hybridization, slides were scanned and analysed using the Feature Extraction software (version A.4.0.45, Agilent Technologies), as recommended by the manufacturer. Spots that did not pass quality control procedures in the Feature Extraction software were flagged and removed from further analysis. Clones with the same GenBank accession number were averaged.

Expression profiling on Agilent cDNA microarrays

Total RNA (20 μg) was reverse transcribed using the Agilent direct-label cDNA synthesis kit (Agilent Technologies), following the manufacturer's directions. Labeled cDNA was purified using QIAquick PCR Purification columns (Qiagen, Valencia, CA, USA), followed by concentration by vacuum centrifugation. cDNA was suspended in hybridization buffer and hybridized to Agilent human 1 cDNA microarrays (Agilent Technologies) for 17 h at 65°C, according to the

Agilent protocol. To avoid generation of false between-group differences by randomly pairing glioma samples on the two-channel cDNA arrays, each sample was individually labeled and co-hybridized with a normal brain sample labeled with a complementary dye. Normal brain samples were generated by pooling equal amounts of RNA from each control sample and labeling as for individual samples. In addition, Cy dye switch hybridizations were performed for each sample. Normal brain samples were purchased from Clontech (Tokyo, Japan). All microarray data and clinical features have been submitted to Gene Expression Omnibus (GEO, http://www.ncbi.nlm.nih.gov/geo; accession no. GSE4381).

Statistical analysis

Univariate analysis for clinical features was performed by log-rank test using SAS software ver. 9.1.3 (SAS Institute Inc., Cary, NC, USA). In microarray analysis, normalization and survival analysis were performed using the BRB Array Tools software ver. 3.3.0 (http://linus.nci.nih.gov/BRB-ArrayTools.html) developed by Dr Richard Simon and Amy Peng. In brief, a log base 2 transformation was applied to the microarray raw data, and global normalization was used to median the center of log ratios on each array in order to adjust for differences in labeling intensities of the Cy3 and Cy5 dyes. Genes showing minimal variation across the set of arrays were excluded from the analysis. Genes whose expression differed by at least 1.5-fold from the median in at least 20% of the arrays were retained. Genes were also excluded if percent of data missing or filtered out exceeds 50%. Then, genes that passed filtering criteria were considered for further analysis.

We computed a statistical significance level for each gene based on univariate proportional hazards models ($P<0.005$) and identified genes whose expression was significantly related to survival of the patient. These *P*-values were then used in a multivariate permutation test in which survival times and censoring indicators were randomly permuted among arrays. To adjust the expression of six candidate genes (DDR1, DYRK3, KSP37, ITGA5, SLN and ALCAM) for clinical features (WHO grade, age, gender, PS), clinical data and normalized microarray expression data of six genes were imported into SAS software ver. 9.1.3 (SAS Institute Inc.) and Cox regression model was performed for multivariate analysis against each variable (WHO grade, age, gender, PS, expression levels of six genes). Three samples were excluded for multivariate analysis because there were a few defected expression data. A *P*–value <0.05 was considered significant. The differences between subgroups of DDR1 siRNA and control groups were tested for statistical significance using the analysis of variance test and statistical significance was determined at the $P<0.01$ level.

Validation of differential expression by real-time quantitative PCR

Total RNA (2 μg) was subjected to DNase treatment in a 10 μl reaction containing 1 μl 10 × DNase I reaction buffer (Invitrogen, Tokyo, Japan) and 1 μg DNase I at room temperature for 10 min. Ethylenediamine tetraacetic acid (1 μl, 25 mM) and 1 μl oligo dT (0.5 μg/μl; Invitrogen) were added to the DNase reaction, and heated to 70°C for 15 min to inactivate DNase I activity and eliminate RNA secondary structure. Samples were placed on ice for 2 min and collected by brief centrifugation. RNA was then reverse-transcribed into cDNA by adding 8 μl master mix containing 4 μl of 5 × first strand buffer, 2 μl dithiothreitol (0.1 M), 1 μl dNTPs (10 mM each) and 1 μl SuperScript II (200 U/μl) (Invitrogen), followed by incubation at 42°C for 45 min. The reaction was diluted 10-fold with dH_2O and stored at 4°C.

Each sample was subjected to 40 cycles of real-time PCR with a LightCycler (Idaho Technology, Salt Lake City, UT, USA). PCR reagents contained 1 × LightCycler DNA Master SYBR Green I (Roche Molecular Biochemicals, Mannheim, Germany), 0.5 μM of each primer, 3 mM $MgCl_2$ and 2 μl cDNA template. PCR conditions were as follows: one cycle of denaturing at 95°C for 10 min, followed by 40 cycles of 95°C for 15 s, 55°C for 5 s and 72°C for 10 s. A melting curve was obtained at the end of amplification cycles to verify specificity of the PCR products. Points at which signal fluorescence exceeded background, for each sample and for each gene, were compared to a standard curve generated by four, 10-fold serial dilutions of concentrated cDNA control of each sample subjected to real-time analysis to determine an expression value. All determinations were performed in duplicate. A Student's *t*-test was conducted to analyse expression values for long- and short-term survivors to determine statistical significance. For amplification of target genes, the following primers were used (Takara, Yotsukaichi, Japan):

ALCAM-FW:	5′-CCAGATGGCAATATCACATGGTACA-3′,
ALCAM-RW:	5′TCCAGGGTGGAAGTCATGGTATAGA-3′,
DDR1-FW:	5′ACTTTGGCATGAGCCGGAAC-3′,
DDR1-RW:	5′ACGTCACTCGCAGTCGTGAAC-3′,
DYRK3-FW:	5′AGCTGCCTCCAGTTGTTGGGAATAG-3′,
DYRK3-RW:	5′TGCATCTCTGGGCATATCTCTGTC-3′,
ITGA5-FW:	5′TCCCAGTAAGCGACTGGCATC-3′,
ITGA5-RW:	5′GTTCCAGCACACCCTGGCTAA-3′,
ITGB2-FW:	5′ATCGTGCTGATCGGCATTCTC-3′,
ITGB2-RW:	5′GGTTCATGACCGTCGTGGTG-3′,
KSP37-FW:	5′CTTCCGAGGGTGACAGGTGA-3′,
KSP37-RW:	5′TCCAGTGTGAGAACGTTGGATTG-3′,
LDHC-FW:	5′TCATCTGTACTGATTGCGCCAAG-3′,
LDHC-RW:	5′ACGGCACCAGTTCCAACAATAGTAA-3′,
LOC340371-FW:	5′GGAACATGCCAGGGCTTCA-3′,
LOC340371-RW:	5′CTGCTCAACACGGTCTGGA-3′,
SLN-FW:	5′GGAGTTGGAGCTCAAGTTGGAGAC-3′,
SLN-RW:	5′GAACTGCAGGCAGATTTCTGAGG-3′,
SLC2A3-FW:	5′GCCTTTGGCACTCTCAACCAG-3′,
SLC2A3-RW:	5′GCTGCACTTTGTAGGATAGCAGGAA-3′.

Immunohistochemistry

Sections (5 μm) from formalin-fixed, paraffin-embedded tissue specimens were deparaffinized in xylene and dehydrated in a graded series of ethanol, followed by a phosphate-buffered saline (PBS) wash. Antigen retrieval was carried out by incubation at 121°C for 10 min in 10 mM sodium citrate (pH 6.0), followed by incubation with 0.3% H_2O_2 to quench endogenous peroxidase activity. Slides were blocked in 10% normal serum and incubated with rabbit polyclonal anti-DDR1 antibody (dilution 1:50; Santa Cruz Biotechnology, Santa Cruz, CA, USA) for 16 h at 4°C. After washing, the slides were incubated with an avidin–biotin–peroxidase system (Vectastain elite ABC kit, Vector Labs, Burlingame, CA,

USA). Finally, sections were exposed for 10–20 min to 0.01% 3,3-diaminobenzidine (Sigma, Tokyo, Japan) and PBS containing 0.01% hydrogen peroxide. Immunohistochemistry scoring was performed as follows. Staining intensity was classified as none (0 point), weak (1 point), moderate (2 point) or strong (3 point). Intensity of signal of stained areas was estimated by light microscopy, based on 25 percentiles in a representative field. Scores were calculated as weighted averages (sum of points × area%). Averages of three independent measurements were calculated to the first decimal place and used for statistical analysis. Observers were not aware of case numbers.

siRNA treatment and cell proliferation assay

Specific siRNA oligonucleotides directed against human DDR1 were purchased from Invitrogen. The Validated Stealth sequence information is DDR1-#1: 5′-GCUAUGUGGAGAU GGAGUUUGAGUU-3′ and DDR1-#2: 5′-GGCCCUGG UUACUCUUCAGCGAAAU-3′. siRNAs were introduced into glioma cell lines by cytofectin-mediated transfection according to the manufacturer's instructions (Qiagen, Tokyo, Japan). Cells were cultured in 96-well plates in 100 μl of serum-enriched medium. When 80% confluence was reached, 25 μl 100 nM siRNA in cytofectin was added drop wise to the cell culture. Numbers of viable cells were evaluated 48 h after culture, by incubating with Tetra color one (Seikagaku CO., Tokyo, Japan), and numbers obtained were compared with those of controls. Control experiments were performed using Cy3-labeled siRNA (Qiagen) directed against an unrelated mRNA (Luciferase; $siRNA_{LUC}$: Qiagen). Transfection efficiency was confirmed with Cy3-labeled $siRNA_{LUC}$ in each assay. All proliferation experiments were repeated as independent experiments at least twice. Results were reported as means ± s.d. of two independent experiments.

Cell invasion of Matrigel

A Transwell containing an 8-μm diameter pore membrane (Becton-Dickinson, Tokyo, Japan) was coated with 500 μl Matrigel (Becton-Dickinson) at 100 μg/ml. Cells were either left untreated, treated with control or DDR1-#1, #2 siRNAs and transfected as described above. After 24-h incubation, cells were detached with cell dissociation solution (Sigma), washed twice with PBS and resuspended in minimum essential medium (MEM) (Nissui Pharmaceutical Inc., Tokyo, Japan) containing 10% fetal bovine serum (FBS) (Gibco, Tokyo, Japan). When siRNAs were used, a second transfection 24 h after the first was performed. In all cases, 2×10^5 cells were seeded into the upper, Matrigel-coated chamber of the Transwell. The lower chamber was filled with MEM supplemented with 10% FBS. After 24-h incubation at 37°C, the non-migrating cells in the upper chamber were gently detached by scraping and adherent cells present on the lower surface of each insert were stained with Giemsa. Ten fields were counted by light microscopy at ×200 magnification. Results were calculated with reference to control values observed after incubation of untreated control, for control and DDR1 siRNA.

Cell lines and culture

All glioma cell lines were cultured in MEM supplemented with 10% FBS. The T98G, GI-1 and U251 cell lines were purchased from Cell Bank, RIKEN BioResource Center (Tsukuba, Japan).

Abbreviations

ALCAM, activated leukocyte cell adhesion molecule; cDNA, complementary DNA; Cy, cyanine; DDR1, discoidin domain receptor family, member 1; DYRK3, dual-specificity tyrosine-(Y)-phosphorylation-regulated kinase 3; FBS, fetal bovine serum; ITGA5, integrin alpha 5; ITGB2, integrin beta 2; KSP37, Ksp37 protein; LDHC, lactate dehydrogenase C; LOC340371, hypothetical protein LOC340371; MEM, minimum essential medium; PBS, phosphate-buffered saline; SLC2A3, solute carrier family 2 member 3; SLN, sarcolipin; s.d., standard deviation; siRNA, short interfering RNA.

Acknowledgements

We are grateful to N Kiyama and F Higuchi for their excellent technical assistance. We thank Dr Rich Simon and Amy Peng for providing the BRB ArrayTools software. The free software was very useful and developed for user-friendly applications. We also thank Tetsutaro Hamano for statistical advices and analysis.

References

Agrawal D, Chen T, Irby R, Quackenbush J, Chambers AF, Szabo M *et al.* (2002). *J Natl Cancer Inst* **94**: 513–521.

Freije WA, Castro-Vargas FE, Fang Z, Horvath S, Cloughesy T, Liau LM *et al.* (2004). *Cancer Res* **64**: 6503–6510.

Godard S, Getz G, Delorenzi M, Farmer P, Kobayashi H, Desbaillets I *et al.* (2003). *Cancer Res* **63**: 6613–6625.

Hoelzinger DB, Mariani L, Weis J, Woyke T, Berens TJ, McDonough WS *et al.* (2005). *Neoplasia* **7**: 7–16.

Hunter SB, Brat DJ, Olson JJ, Von Deimling A, Zhou W, Van Meir EG. (2003). *Int J Oncol* **23**: 857–869.

Karpeh MS, Kelsen DP, Tepper JE. (2001) In: Devita Jr VT (ed) *Cancer of the Stomach: Cancer, Principles & Practice of Oncology*, 6th edn. Lippincott Williams & Wilkins: Philadelphia, pp 1092–1121.

Khan J, Wei JS, Ringner M, Saal LH, Ladanyi M, Westermann F *et al.* (2001). *Nat Med* **7**: 673–679.

Kim S, Dougherty ER, Shmulevich I, Hess KR, Hamilton SR, Trent JM *et al.* (2002). *Mol Cancer Ther* **1**: 1229–1236.

Kleihues P, Cavenee WK. (2000). *World Health Organization Classification of Tumours of the Nervous System*. WHO/IARC: Lyon, France.

Li K, Zhao S, Karur V, Wojchowski DM. (2002). *J Biol Chem* **277**: 47052–47060.

Liang Y, Diehn M, Watson N, Bollen AW, Aldape KD, Nicholas MK *et al.* (2005). *Proc Natl Acad Sci USA* **102**: 5814–5819.

Mischel PS, Cloughesy TF, Nelson SF. (2004). *Nat Rev Neurosci* **5**: 782–792.

Mischel PS, Shai R, Shi T, Horvath S, Lu KV, Choe G *et al.* (2003). *Oncogene* **22**: 2361–2373.

Nigro JM, Misra A, Zhang L, Smirnov I, Colman H, Griffin C *et al.* (2005). *Cancer Res* **65**: 1678–1686.

Nutt CL, Mani DR, Betensky RA, Tamayo P, Cairncross JG, Ladd C *et al.* (2003). *Cancer Res* **63**: 1602–1607.

Ogawa K, Tanaka K, Ishii A, Nakamura Y, Kondo S, Sugamura K *et al.* (2001). *J Immunol* **166**: 6404–6412.

Ramaswamy S, Tamayo P, Rifkin R, Mukherjee S, Yeang CH, Angelo M *et al.* (2001). *Proc Natl Acad Sci USA* **98**: 15149–15154.
Ram R, Lorente G, Nikolich K, Urfer R, Foehr E, Nagavarapu U. (2006). *J Neurooncol* **76**: 239–248.
Rickman DS, Bobek MP, Misek DE, Kuick R, Blaivas M, Kurnit DM *et al.* (2001). *Cancer Res* **61**: 6885–6891.
Rich JN, Hans C, Jones B, Iversen ES, McLendon RE, Rasheed BK *et al.* (2005). *Cancer Res* **65**: 4051–4058.
Sallinen SL, Sallinen PK, Haapasalo HK, Helin HJ, Helen PT, Schraml P *et al.* (2000). *Cancer Res* **60**: 6617–6622.
Shai R, Shi T, Kremen TJ, Horvath S, Liau LM, Cloughesy TF *et al.* (2003). *Oncogene* **22**: 4918–4923.
Sorlie T, Tibshirani R, Parker J, Hastie T, Marron JS, Nobel A *et al.* (2003). *Proc Natl Acad Sci USA* **100**: 8418–8423.
Somasundaram K, Reddy SP, Vinnakota K, Britto R, Subbarayan M, Nambiar S *et al.* (2005). *Oncogene* **24**: 7073–7083.
Stewart LA. (2002). *Lancet* **359**: 1011–1018.
Stupp R, Mason WP, van den Bent MJ, Weller M, Fisher B, Taphoorn MJ *et al.* (2005). *N Engl J Med* **352**: 987–996.
van de Vijver MJ, He YD, van't Veer LJ, Dai H, Hart AA, Voskuil DW *et al.* (2002). *N Engl J Med* **347**: 1999–2009.
van't Veer LJ, Dai H, van de Vijver MJ, He YD, Hart AA, Mao M *et al.* (2002). *Nature* **415**: 530–536.
van den Boom J, Wolter M, Kuick R, Misek DE, Youkilis AS, Wechsler DS *et al.* (2003). *Am J Pathol* **163**: 1033–1043.
Vogel W. (1999). *FASEB J* **13**: S77–82.
Vogel W, Brakebusch C, Fassler R, Alves F, Ruggiero F, Pawson T. (2000). *J Biol Chem* **275**: 5779–5784.
Weiner HL, Zagzag D. (2000). *Cancer Invest* **18**: 544–554.
Wong KK, Chang YM, Tsang YT, Perlaky L, Su J, Adesina A *et al.* (2005). *Cancer Res* **65**: 76–84.
Yoshimura T, Matsuyama W, Kamohara H. (2005). *Immunol Res* **31**: 219–230.

Biochem. J. (2006) 397, 537–543 (Printed in Great Britain) doi:10.1042/BJ20051962

In-frame deletion in the EGF receptor alters kinase inhibition by gefitinib

Kazuko SAKAI*†, Hideyuki YOKOTE‡, Kimiko MURAKAMI-MUROFUSHI†, Tomohide TAMURA§, Nagahiro SAIJO§ and Kazuto NISHIO*‡[1]

*Shien-Lab, National Cancer Center Research Institute, Tsukiji 5-1-1, Chuo-ku, Tokyo 104-0045, Japan, †Department of Biology, Faculty of Science, Ochanomizu University, 2-1-1 Ohtsuka, Tokyo 112-8610, Japan, ‡Pharmacology Division, National Cancer Center Research Institute, Tsukiji 5-1-1, Chuo-ku, Tokyo 104-0045, Japan, and §Medical Oncology, National Cancer Center Hospital, National Cancer Center Research Institute, Tsukiji 5-1-1, Chuo-ku, Tokyo 104-0045, Japan

The existence of an in-frame deletion mutant correlates with the sensitivity of lung cancers to EGFR (epidermal growth factor receptor)-targeted tyrosine kinase inhibitors. We reported previously that the in-frame 15-bp deletional mutation (delE746–A750 type deletion) was constitutively active in cells. Kinetic parameters are important for characterizing an enzyme; however, it remains unclear whether the kinetic parameters of deletion mutant EGFR are similar to those of wild-type EGFR. We analysed autophosphorylation in response to ATP and inhibition of gefitinib for deletion mutant EGFR and wild-type EGFR. Kinetic studies, examining autophosphorylation, were carried out using EGFR fractions extracted from 293-pΔ15 and 293-pEGFR cells transfected with deletion mutant EGFR and wild-type EGFR respectively. We demonstrated the difference in activities between unstimulated wild-type (K_m for ATP $= 4.0 \pm 0.3$ μM) and mutant EGFR (K_m for ATP $= 2.5 \pm 0.2$ μM). There was no difference in K_m values between EGF-stimulated wild-type EGFR (K_m for ATP $= 1.9 \pm 0.1$ μM) and deletion mutant EGFR (K_m for ATP $= 2.2 \pm 0.2$ μM). These results suggest that mutant EGFR is active without ligand stimulation. The K_i value for gefitinib of the deletion mutant EGFR was much lower than that of wild-type EGFR. These results suggest that the deletion mutant EGFR has a higher affinity for gefitinib than wild-type EGFR.

Key words: autophosphorylation, epidermal growth factor receptor (EGFR), gefitinib, kinase inhibition, tyrosine kinase.

INTRODUCTION

EGFR [EGF (epidermal growth factor) receptor] is among the most important targets for lung cancer therapy, and many EGFR-targeted inhibitors have been developed [1]. These EGFR-targeted compounds inhibit the tyrosine kinase activity of EGFR by competing at the ATP-binding site [2]. Many EGFR-targeted tyrosine kinase inhibitors such as gefitinib and erlotinib have been assessed clinically [3,4]. Recently, an EGFR mutation was found in patients who responded to gefitinib, and mutant EGFR has been reported to be a determinant of the response to EGFR tyrosine kinase inhibitors [5,6]. To date, over 30 EGFR mutations including delE746–A750, L858R and delL747–P753insS, have been reported in lung cancer. These EGFR mutations, except for T790M, are considered to be of the 'gain-of-function' type. Differences exist among them; for example, constitutively active in delE746–A750 compared with hyperresponsive to ligand stimulation in L858R and delL747–P753insS, although these mutant EGFRs increase sensitivity to EGFR-targeted tyrosine kinase inhibitors [7–9]. In general, the observation of hyperresponsiveness to ligand stimulation, as in the case of L858R, raises the possibility of high affinity for ATP. We reported previously that deletion mutant EGFR was constitutively phosphorylated under unstimulated conditions, whereas wild-type EGFR was not phosphorylated until ligand stimulation [7]. The differences in cellular phenotype and sensitivity to gefitinib between deletion mutant EGFR and wild-type EGFR raise the possibility that the enzymatic properties of the deletion mutant EGFR may differ from those of wild-type EGFR. However, it remains unclear whether the kinetic parameters of deletion mutant EGFR are different from those of wild-type EGFR. In the present study, we focused on the autophosphorylation of deletion mutant EGFR, and investigated the inhibition constant of gefitinib. Technically, we used deletion mutant EGFR and wild-type EGFR extracted from ectopically expressed HEK-293 (human embryonic kidney) cells. The autophosphorylation assay reflects the native behaviour of EGFR in maintaining cellular functions.

MATERIALS AND METHODS

Reagents

Gefitinib (Iressa®, ZD1839) was provided by AstraZeneca.

Cell culture

The HEK-293 cell line was obtained from the A.T.C.C. (Manassas, VA, U.S.A.) and was cultured in RPMI 1640 medium (Sigma) supplemented with 10% heat-inactivated foetal bovine serum (Life Technologies).

Plasmid construction and transfection

Construction of the expression plasmid vector of wild-type EGFR and the 15-bp deletion mutant EGFR (delE746–A750 type deletion), which has the same deletion site as that observed in detail in PC-9 cells, has been described elsewhere [7,10,11]. The plasmids were transfected into HEK-293 cells and the transfectants were selected using Zeosin (Sigma). The stable transfectants (pooled cultures) of the wild-type EGFR and its deletion mutant were designated 293-pEGFR and 293-pΔ15 cells respectively.

Abbreviations used: EGF, epidermal growth factor; EGFR, EGF receptor; HEK-293, human embryonic kidney; 293-pEGFR, HEK-293 cells transfected with wild-type EGFR; 293-pΔ15, HEK-293 cells transfected with deletion mutant EGFR; TBS-T, Tris-buffered saline with Tween 20; TGF-α, transforming growth factor-α.

[1] To whom correspondence should be addressed (email knishio@gan2.res.ncc.go.jp).

Immunoblotting

The 293-pΔ15 and 293-pEGFR cells were treated with or without gefitinib for 3 h, stimulated with EGF (100 ng/ml) under serum-starvation conditions and then lysed for immunoblot analysis. Immunoblot analysis was performed as described previously [12]. Equivalent amounts of protein were separated by SDS/PAGE (2–15 % gradient) and transferred to a PVDF membrane (Millipore). The membrane was probed with a mouse monoclonal antibody against EGFR (Transduction Laboratories), a phospho-EGFR antibody (specific for Tyr^{1068}) (Cell Signaling Technology) as the first antibody, followed by a horseradish-peroxidase-conjugated secondary antibody. The bands were visualized with ECL® (enhanced chemiluminescence) (Amersham Biosciences).

Determination of ligand secretion by ELISA

The 293-pΔ15 and 293-pEGFR cells were cultured in 12-well plates under serum-starvation conditions. The cell culture supernatant was collected for each cell line and stored at −80 °C for further analysis. Amounts of EGF and TGF-α (transforming growth factor α) in the culture medium from each cell line were determined with a DuoSet ELISA development kit (R&D Systems). The assay was performed in triplicate according to the manufacturer's instructions.

Preparation of cell lysates for EGFR autophosphorylation

Cultivated cells, after reaching 70–80 % confluence, were starved in serum-free medium for 24 h, with or without EGF (100 ng/ml) stimulation. The cells were washed twice with ice-cold PBS containing 0.33 mM $MgCl_2$ and 0.9 mM $CaCl_2$ [PBS(+)], then lysed with lysis buffer [50 mM Tris/HCl, pH 7.4, 50 mM NaCl, 0.25 % Triton X-100, 5 mM EDTA, protease inhibitor (Roche Diagnostics) and phosphatase inhibitor (Sigma)]. For the preparation of gefitinib-treated cell lysates, cultivated cells were starved in serum-free medium for 24 h, and were then pre-incubated with 2 μM gefitinib for 3 h. Either with or without EGF stimulation (100 ng/ml), the cells were washed twice with ice-cold PBS(+) and lysed with lysis buffer. The cell lysate was centrifuged at 20000 *g* for 10 min, and the protein concentration of the supernatant was measured with a BCA (bicinchoninic acid) protein assay (Pierce).

Autophosphorylation assay

The amount of EGFR in 293-pΔ15 and 293-pEGFR cells was determined by quantitative immunoassay (R&D Systems) according to the manufacturer's instructions. The autophosphorylation assay was carried out with a quantitative immunoassay system. Wells in a 96-well immunomodule (Nalge Nunc International) were incubated with 0.8 μg/ml goat anti-(human EGFR) antibody in PBS (provided with the EGFR quantitative immunoassay system) and incubated at 4 °C overnight. The plates were washed three times with TBS-T (Tris-buffered saline with Tween 20; 20 mM Tris/HCl, pH 7.4, 150 mM NaCl and 0.05 % Tween 20) and were then filled with blocking buffer (PBS containing 1 % BSA and 5 % sucrose) and incubated for 2 h at room temperature (25 °C). The wells were washed three times with TBS-T and incubated with cell lysates of 293-pEGFR or 293-pΔ15 including equal amounts of EGFR (130 ng of EGFR/well) diluted with lysis buffer. After a 2 h incubation at room temperature, the 96-well plate was washed with TBS-T. Autophosphorylation of EGFR was initiated by addition of ATP (0–32 μM in 50 mM Tris/HCl, pH 7.5, 20 mM $MgCl_2$ and phosphatase inhibitor) followed by incubation for 5 min. In some experiments, various concentrations of gefitinib were added to the wells before the addition of ATP. Following the autophosphorylation reaction, the wells were washed with TBS-T. Next,

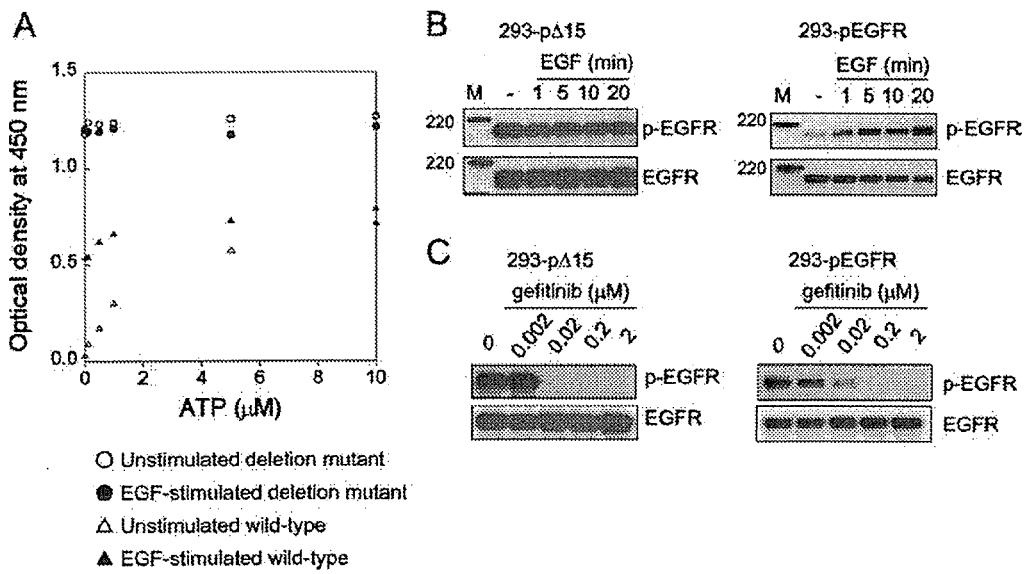

Figure 1 Autophosphorylation reactions of deletion mutant EGFR and wild-type EGFR

(**A**) The 293-pΔ15 and 293-pEGFR cells were treated with or without EGF (100 ng/ml) for 10 min after serum-starvation. EGFR was extracted from the cells and immobilized on wells with anti-EGFR antibody. Autophosphorylation reactions were initiated by the addition of ATP, and autophosphorylation was detected using horseradish-peroxidase-conjugated phosphotyrosine antibody, measuring the absorbance ('optical density') at 450 nm. Autophosphorylation was seen for unstimulated (○) and EGF-stimulated (●) deletion mutant EGFR, and unstimulated (△) and EGF-stimulated (▲) wild-type EGFR. Results are representative of at least three independent experiments. (**B**) The 293-pΔ15 and 293-pEGFR cells were treated with or without EGF (100 ng/ml) for the indicated times after serum-starvation. Phosphorylation of EGFR and total EGFR was determined by immunoblotting. (**C**) The 293-pΔ15 and 293-pEGFR cells were exposed to gefitinib (0.002–2 μM) for 3 h under serum-starvation conditions, and stimulated with EGF (100 ng/ml) for 10 min. The cells were then lysed and subjected to immunoblot analysis.

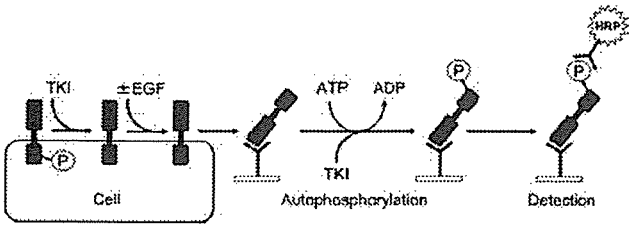

Figure 2 Schematic illustration of the cell-based autophosphorylation assay

The 293-pΔ15 and the 293-pEGFR cells overexpressing deletion mutant EGFR and wild-type EGFR respectively were treated with 2 μM gefitinib for 3 h and stimulated with or without EGF (100 ng/ml) under serum-starvation conditions. EGFR was extracted from cells and immobilized on wells with anti-EGFR antibody. The autophosphorylation reaction was initiated by the addition of ATP with or without gefitinib, and horseradish-peroxidase-conjugated anti-phosphotyrosine antibody was used to detect the phosphorylation of EGFR. TKI, tyrosine kinase inhibitor.

horseradish-peroxidase-conjugated anti-phosphotyrosine antibody, PY-99-HRP (0.4 μg/ml in PBS containing 1% BSA and 0.1% Tween 20) (Santa Cruz Biotechnology) was added to the wells for 2 h at room temperature. The wells were washed three times with TBS-T. Bound phosphotyrosine antibody was detected colorimetrically after adding 100 μl of substrate (tetramethylbenzidine and H_2O_2) to each well. After a 10 min incubation, the colour reaction was quenched by the addition of 100 μl of 1M H_2SO_4. The absorbance readings for each well were determined at 450 nm with Delta-soft on an Apple Macintosh computer interfaced to a Bio-Tek Microplate Reader EL-340 (BioMetallics).

Data analysis

For kinetic analysis, an Eadie–Hofstee plot was applied for the calculation of K_m (Michaelis constant) and V_{max} (maximum velocity). The data obtained were plotted as velocity against velocity/substrate concentration (V/ATP). The slope of the line is equal to $-K_m$ and the x-intercept is V_{max}. The K_i value was calculated as follows:

$$K_i = (K_m \times [I])/(K_{m,I} - K_m) \quad (1)$$

in which K_m is the Michaelis constant for ATP, $K_{m,I}$ is the Michaelis constant for ATP in the presence of gefitinib and [I] is the concentration of gefitinib. The statistical analysis was performed using KaleidaGraph (Synergy Software).

RESULTS

Autophosphorylation of deletion mutant EGFR and wild-type EGFR

We performed the autophosphorylation assay and immunoblot analysis using lysates extracted from 293-pΔ15 and 293-pEGFR cells under unstimulated and EGF-stimulated conditions (Figures 1A and 1B). Under unstimulated conditions, deletion mutant EGFR was highly phosphorylated in the absence of ATP. Addition of ATP did not affect the autophosphorylation of deletion mutant EGFR. On the other hand, autophosphorylation of wild-type EGFR was barely detectable without ATP, and proceeded in an ATP-dependent manner. In the EGF-stimulated case, wild-type EGFR was phosphorylated to a greater extent in the absence of ATP than unstimulated wild-type EGFR. The autophosphorylation of EGF-stimulated wild-type EGFR additively increased with the addition of ATP. These findings indicate that the deletion mutant retains the constitutive activity in our autophosphorylation assay. In the immunoblot analysis, phosphorylation of deletion mutant EGFR was detected in 293-pΔ15 cells without ligand stimulation. Addition of EGF increased phosphorylation of EGFR in the 293-pEGFR cells. Taken together, these results indicate that the deletion mutant has constitutive autophosphorylation activity.

In addition, we examined the secretion of major ligands for EGFR such as EGF and TGF-α from transfected HEK-293 cells by ELISA. No detectable EGF and TGF-α secretion was observed in the cultivation medium used for HEK-293 transfectants (results not shown), indicating that these transfectants are not activated via EGF-mediated autocrine loops. We considered that autophosphorylation using unstimulated EGFR represents a

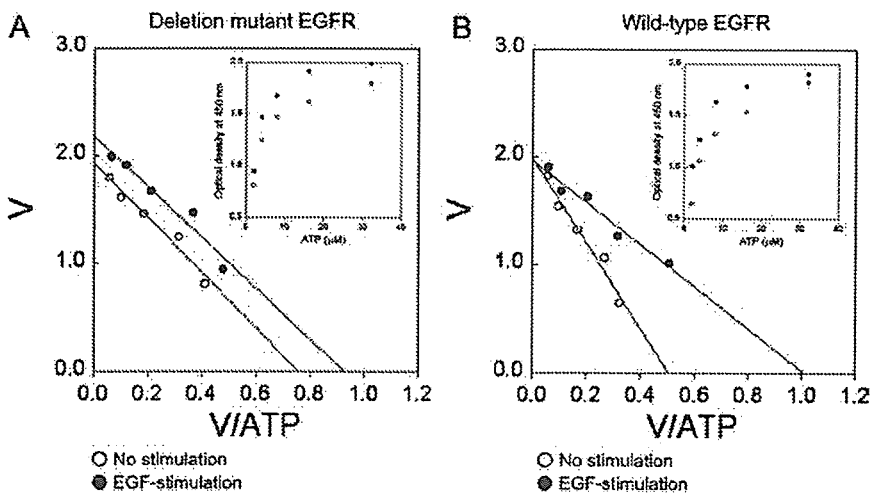

Figure 3 Autophosphorylation activities of deletion mutant EGFR and wild-type EGFR

Plots of absorbance ('optical density') against ATP concentration (inset) were fitted to an Eadie–Hofstee plot to calculate the values of kinetic parameters (K_m and V_{max}) for deletion mutant EGFR (**A**) and wild-type EGFR (**B**) under unstimulated (○) and EGF-stimulated conditions (●). Results are representative of at least three independent experiments with similar results.

Table 1 Kinetic parameters for ATP

The autophosphorylation reaction was performed using the indicated enzyme and gefitinib (0.5–5 nM). The steady-state kinetic parameters for ATP were determined from the Eadie–Hofstee plot in Figure 5. Results are means ± S.D. for three independent duplicate experiments.

		K_m (μM)				V_{max} (μM · min^{-1})			
		Deletion mutant		Wild-type		Deletion mutant		Wild-type	
Gefitinib (nM)	EGF stimulation...	−	+	−	+	−	+	−	+
0		2.5 ± 0.2	2.2 ± 0.2	4.0 ± 0.3	1.9 ± 0.1	1.9 ± 0.1	2.1 ± 0.1	2.0 ± 0.0	1.9 ± 0.0
0.5		5.6 ± 0.5	5.7 ± 0.4	4.1 ± 0.4	2.3 ± 0.1	1.9 ± 0.1	1.9 ± 0.2	2.0 ± 0.1	1.9 ± 0.1
1		9.8 ± 2.8	10.9 ± 3.0	4.6 ± 1.2	2.5 ± 0.1	2.0 ± 0.1	1.9 ± 0.0	2.0 ± 0.2	1.8 ± 0.1
5		26.1 ± 5.4	30.2 ± 4.2	7.0 ± 2.3	4.9 ± 0.9	1.9 ± 0.1	1.8 ± 0.2	2.0 ± 0.1	1.8 ± 0.2

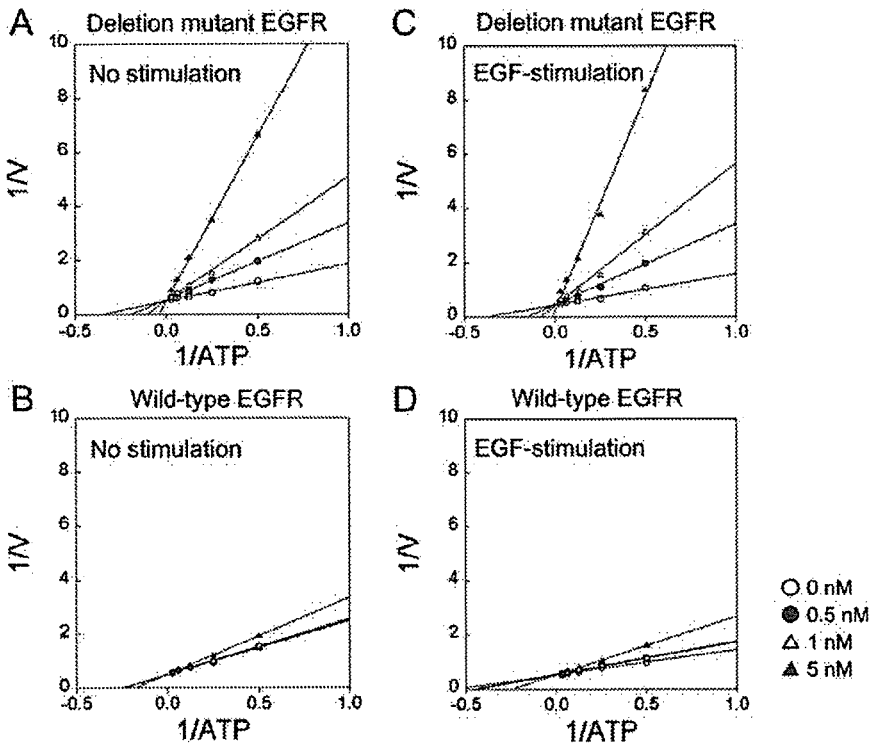

Figure 4 Mechanism of inhibition of deletion mutant EGFR by gefitinib

Autophosphorylation of unstimulated deletion mutant (**A**), unstimulated wild-type (**B**), EGF-stimulated deletion mutant (**C**) and EGF-stimulated wild-type (**D**) EGFR was measured with or without gefitinib at concentrations of 0 (○), 0.5 (●), 1 (△) and 5 (▲) nM. Reciprocal velocity against reciprocal ATP concentrations (0.5–32 μM) were plotted. Data are representative of at least three independent experiments.

low level of EGF-independent basal phosphorylation, whereas autophosphorylation using EGF-stimulated EGFR represents EGF-induced phosphorylation.

Kinetic parameters of autophosphorylation

The deletion mutant EGFR is constitutively phosphorylated under unstimulated conditions. Measuring the autophosphorylation activity of deletion mutant EGFR requires unphosphorylated tyrosine residues of EGFR. An autophosphorylation assay was reconstructed to determine the kinetic parameters of deletion mutant EGFR. The method is summarized in Figure 2. The concentrations of gefitinib used (2 μM) completely inhibited phosphorylation of both the deletion mutant and wild-type EGFR, as demonstrated by immunoblot analysis (Figure 1C). We performed autophosphorylation assays with various amounts of EGFR (results not shown). In our autophosphorylation assay, a constant amount of EGFR (130 ng/well) was adopted to measure its autophosphorylation, because this amount of EGFR was found to be appropriate for detecting changes in the absorbance of both wild-type and deletion mutant EGFR. The autophosphorylation of deletion mutant EGFR and wild-type EGFR was analysed by comparison with unstimulated and EGF-stimulated EGFR (Figure 3). The higher phosphorylation of deletion mutant EGFR shown in Figure 1(A) was lowered by using gefitinib-treated lysates, while the autophosphorylation reaction was initiated by addition of ATP. The ATP-dependent autophosphorylation reactions of deletion mutant EGFR and wild-type EGFR in crude cellular extracts were monitored (Figure 3, insets). The data were transformed into an Eadie–Hofstee plot, and the kinetic parameters were determined as apparent K_m and V_{max} values for ATP (Figure 3 and Table 1). Under unstimulated conditions,

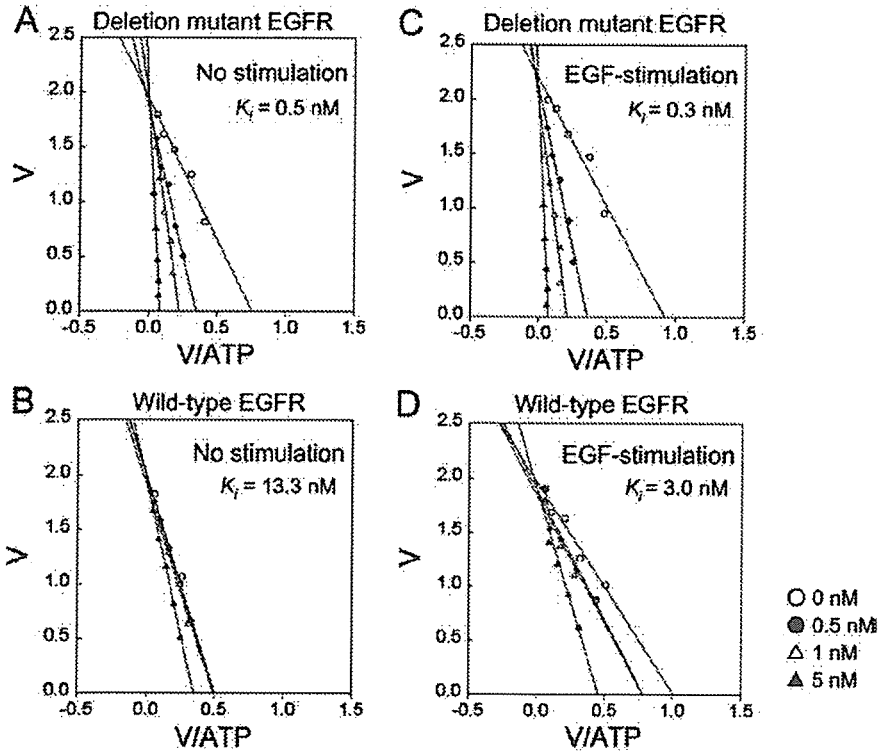

Figure 5 Inhibition constant of gefitinib for autophosphorylation activity of deletion mutant EGFR

The same dataset as shown in Figure 4 was fitted to an Eadie–Hofstee plot, and kinetic parameters from this fit are summarized in Table 1. Shown are the results for the unstimulated (**A**) and EGF-stimulated (**C**) deletion mutant EGFR and unstimulated (**B**) and EGF-stimulated (**D**) wild-type EGFR in response to ATP with or without gefitinib at concentrations of 0 (○), 0.5 (●), 1 (△) and 5 (▲) nM. Results are representative of at least three independent experiments.

differences in activities were seen between unstimulated wild-type (K_m for ATP = 4.0 ± 0.3 μM) and deletion mutant EGFR (K_m for ATP = 2.5 ± 0.2 μM). Under EGF-stimulated conditions, there was no difference in K_m values between EGF-stimulated wild-type EGFR (K_m for ATP = 1.9 ± 0.1 μM) and deletion mutant EGFR (K_m for ATP = 2.2 ± 0.2 μM). The V_{max} values of wild-type EGFR and deletion mutant EGFR were equal under both conditions. These results suggest that the wild-type EGFR is conformationally activated by EGF stimulation, and that the mutant EGFR is active without ligand stimulation.

Gefitinib inhibits autophosphorylation of deletion mutant EGFR

We examined the inhibitory effect of gefitinib (0.5, 1 and 5 nM) on the autophosphorylation of deletion mutant EGFR in comparison with wild-type EGFR under unstimulated and EGF-stimulated conditions. The data were transformed into a Lineweaver–Burk plot for estimation of the mode of inhibition (Figure 4). Lineweaver–Burk plot analysis showed that gefitinib competitively inhibited the autophosphorylation of deletion mutant EGFR as well as that of wild-type EGFR. The data were transformed into an Eadie–Hofstee plot for determination of kinetic parameters (Figure 5). Eadie–Hofstee plot analysis revealed the apparent K_m and V_{max} values for ATP in the presence of various gefitinib concentrations, and the kinetic parameters are summarized in Table 1. The K_i for deletion mutant EGFR and wild-type EGFR was calculated using eqn 1 (see the Materials and methods section). The K_i value of gefitinib for deletion mutant EGFR (K_i for gefitinib = 0.5 ± 0.1 nM) was 26-fold lower than that for wild-type EGFR (K_i for gefitinib = 13.3 ± 5.1 nM) under unstimulated conditions (Figure 5). Under EGF-stimulated conditions, the K_i value of gefitinib for deletion mutant EGFR (0.3 ± 0.1 nM) was 10-fold lower than that for wild-type EGFR (3.0 ± 0.6 nM) (Figure 5). Based on these comparative studies, we concluded that gefitinib binds deletion mutant EGFR more strongly than wild-type EGFR. In addition, we calculated the inhibitory effect of gefitinib for both types of EGFR in the presence of 2 μM ATP (Figure 6). Relatively strong inhibitory activity was detected for deletion mutant EGFR as compared with wild-type EGFR. These results suggest that gefitinib had a high affinity (low K_i value) for deletion mutant EGFR compared with wild-type EGFR.

DISCUSSION

Wild-type EGFR is unphosphorylated, being in an inactive form, under unstimulated conditions. The binding of ligands to the extracellular domain of EGFR induces dimerization and phosphorylation of the receptor into the active form [13]. The kinetic parameters of wild-type EGFR in our autophosphorylation assay are consistent with those of previous reports [14,15]. Crystallographic analysis has shown that the structure of the EGFR kinase domain after forming a complex with erlotinib exhibits a conformation consistent with the active form of protein kinases [16,17]. Previously, we reported that the deletion mutant EGFR was dimerized and phosphorylated constitutively without ligand stimulation, suggesting an active conformation [9]. We analysed the enzymatic properties of the deletion mutant EGFR, and

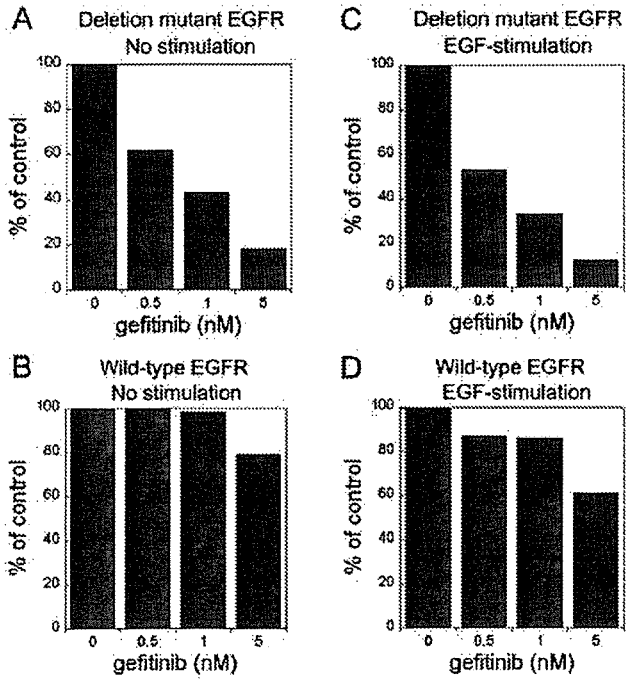

Figure 6 Effects of gefitinib on autophosphorylation of deletion mutant EGFR

The percentage of absorbance compared with the control under conditions of 2 μM ATP was calculated using the same dataset as shown in Figure 4 at a concentration of 2 μM ATP. The results shown are for unstimulated (**A**) and EGF-stimulated (**C**) deletion mutant EGFR and unstimulated (**B**) and EGF-stimulated (**D**) wild-type EGFR in response to ATP with or without gefitinib. Results are representative of at least three independent experiments.

determined the K_i value of gefitinib for deletion mutant EGFR. The inhibition constant of gefitinib for wild-type EGFR was similar to the value reported by Wakeling et al. [18]. We showed that the K_i value of gefitinib for deletion mutant EGFR was much lower than that for wild-type EGFR. The evidence of the decreased K_i value of gefitinib for deletion mutant EGFR means that gefitinib binds deletion mutant EGFR more strongly than wild-type EGFR. The high-affinity interaction between deletion mutant EGFR and gefitinib may be attributable to structural differences between deletion mutant EGFR and wild-type EGFR.

Our conclusion does not contradict the previous report by Stamos et al. [16] on a similar EGFR-targeted tyrosine kinase inhibitor, erlotinib, which binds to the active form of EGFR [14]. This result differs from that reported elsewhere: Fabian et al. [19] reported that there were no differences in the binding affinity of EGFR-targeted tyrosine kinase inhibitors between wild-type EGFR and mutant EGFR, including the deletion mutation. They constructed and expressed the kinase domain of EGFR on a bacteriophage surface, followed by interaction with immobilized inhibitors using biotin–avidin systems. Conversely, in our experiments, we performed autophosphorylation assays with EGFR extracted from 293-pΔ15 and the 293-pEGFR cells overexpressing deletion mutant and wild-type EGFR respectively. We consider our cell-based autophosphorylation assay results to reflect the native state of deletion mutant EGFR and to possibly explain the hypersensitivity of mutant-expressing cells to gefitinib.

We demonstrated that the deletion mutant actually binds gefitinib more strongly than wild-type EGFR. This is likely to be the mechanism of action of other tyrosine kinase inhibitors such as erlotinib, ZD6474 [dual inhibitor targeted to VEGFR2 (vascular endothelial growth factor receptor 2)/KDR (kinase insert domain-containing receptor) and EGFR] and other possible multi-targeted tyrosine kinase inhibitors. Indeed, EGFR-specific tyrosine kinase inhibitors AG1478 and erlotinib, as well as ZD6474, as described in our previous report [7] showed different growth-inhibitory activities against HEK-293 transfected with deletion mutant EGFR (results not shown). Thus it is likely that these (ATP competitive) tyrosine kinase inhibitors have different binding property effects on wild-type and deletion mutant EGFR to those of gefitinib.

In the present study, we focused on the enzymatic properties of in-frame deletion mutant EGFR (delE746–A750). The inhibition of receptor autophosphorylation in deletion mutant EGFR by gefitinib was much greater than that in wild-type EGFR. Next, it is necessary to examine the kinetic properties of other types of EGFR mutants, especially L858R, and these findings may pave the way for the discovery of different kinase inhibitors with different inhibition profiles for EGFR.

This work was supported by funds for the Third Term Comprehensive 10-Year Strategy for Cancer Control.

REFERENCES

1 Arteaga, C. L. (2003) ErbB-targeted therapeutic approaches in human cancer. Exp. Cell Res. **284**, 122–130
2 Traxler, P., Furet, P., Mett, H., Buchdunger, E., Meyer, T. and Lydon, N. (1997) Design and synthesis of novel tyrosine kinase inhibitors using a pharmacophore model of the ATP-binding site of the EGF-R. J. Pharm. Belg. **52**, 88–96
3 Shepherd, F. A., Rodrigues Pereira, J., Ciuleanu, T., Tan, E. H., Hirsh, V., Thongprasert, S., Campos, D., Maoleekoonpiroj, S., Smylie, M., Martins, R. et al. (2005) Erlotinib in previously treated non-small-cell lung cancer. N. Engl. J. Med. **353**, 123–132
4 Bell, D. W., Lynch, T. J., Haserlat, S. M., Harris, P. L., Okimoto, R. A., Brannigan, B. W., Sgroi, D. C., Muir, B., Riemenschneider, M. J., Iacona, R. B. et al. (2005) Epidermal growth factor receptor mutations and gene amplification in non-small-cell lung cancer: molecular analysis of the IDEAL/INTACT gefitinib trials. J. Clin. Oncol. **23**, 8081–8092
5 Lynch, T. J., Bell, D. W., Sordella, R., Gurubhagavatula, S., Okimoto, R. A., Brannigan, B. W., Harris, P. L., Haserlat, S. M., Supko, J. G., Haluska, F. G. et al. (2004) Activating mutations in the epidermal growth factor receptor underlying responsiveness of non-small-cell lung cancer to gefitinib. N. Engl. J. Med. **350**, 2129–2139
6 Paez, J. G., Janne, P. A., Lee, J. C., Tracy, S., Greulich, H., Gabriel, S., Herman, P., Kaye, F. J., Lindeman, N., Boggon, T. J. et al. (2004) EGFR mutations in lung cancer: correlation with clinical response to gefitinib therapy. Science **304**, 1497–1500
7 Arao, T., Fukumoto, H., Takeda, M., Tamura, T., Saijo, N. and Nishio, K. (2004) Small in-frame deletion in the epidermal growth factor receptor as a target for ZD6474. Cancer Res. **64**, 9101–9104
8 Tracy, S., Mukohara, T., Hansen, M., Meyerson, M., Johnson, B. E. and Janne, P. A. (2004) Gefitinib induces apoptosis in the EGFRL858R non-small-cell lung cancer cell line H3255. Cancer Res. **64**, 7241–7244
9 Sakai, K., Arao, T., Shimoyama, T., Murofushi, K., Sekijima, M., Kaji, N., Tamura, T., Saijo, N. and Nishio, K. (2005) Dimerization and the signal transduction pathway of a small in-frame deletion in the epidermal growth factor receptor. FASEB J. **20**, 311–313
10 Nishio, K., Arioka, H., Ishida, T., Fukumoto, H., Kurokawa, H., Sata, M., Ohata, M. and Saijo, N. (1995) Enhanced interaction between tubulin and microtubule-associated protein 2 via inhibition of MAP kinase and CDC2 kinase by paclitaxel. Int. J. Cancer **63**, 688–693
11 Kawamura-Akiyama, Y., Kusaba, H., Kanzawa, F., Tamura, T., Saijo, N. and Nishio, K. (2002) Non-cross resistance of ZD0473 in acquired cisplatin-resistant lung cancer cell lines. Lung Cancer **38**, 43–50
12 Koizumi, F., Shimoyama, T., Taguchi, F., Saijo, N. and Nishio, K. (2005) Establishment of a human non-small cell lung cancer cell line resistant to gefitinib. Int. J. Cancer **116**, 36–44
13 Tanner, K. G. and Kyte, J. (1999) Dimerization of the extracellular domain of the receptor for epidermal growth factor containing the membrane-spanning segment in response to treatment with epidermal growth factor. J. Biol. Chem. **274**, 35985–35990
14 Nair, N., Davis, R. J. and Robinson, H. L. (1992) Protein tyrosine kinase activities of the epidermal growth factor receptor and ErbB proteins: correlation of oncogenic activation with altered kinetics. Mol. Cell. Biol. **12**, 2010–2016

15 Wood, E. R., Truesdale, A. T., McDonald, O. B., Yuan, D., Hassell, A., Dickerson, S. H., Ellis, B., Pennisi, C., Horne, E., Lackey, K. et al. (2004) A unique structure for epidermal growth factor receptor bound to GW572016 (Lapatinib): relationships among protein conformation, inhibitor off-rate, and receptor activity in tumor cells. Cancer Res. **64**, 6652–6659
16 Stamos, J., Sliwkowski, M. X. and Eigenbrot, C. (2002) Structure of the epidermal growth factor receptor kinase domain alone and in complex with a 4-anilinoquinazoline inhibitor. J. Biol. Chem. **277**, 46265–46272
17 Noble, M. E., Endicott, J. A. and Johnson, L. N. (2004) Protein kinase inhibitors: insights into drug design from structure. Science **303**, 1800–1805
18 Wakeling, A. E., Guy, S. P., Woodburn, J. R., Ashton, S. E., Curry, B. J., Barker, A. J. and Gibson, K. H. (2002) ZD1839 (Iressa): an orally active inhibitor of epidermal growth factor signaling with potential for cancer therapy. Cancer Res. **62**, 5749–5754
19 Fabian, M. A., Biggs, 3rd, W. H., Treiber, D. K., Atteridge, C. E., Azimioara, M. D., Benedetti, M. G., Carter, T. A., Ciceri, P., Edeen, P. T., Floyd, M. et al. (2005) A small molecule-kinase interaction map for clinical kinase inhibitors. Nat. Biotechnol. **23**, 329–336

Received 12 December 2005/3 April 2006; accepted 20 April 2006
Published as BJ Immediate Publication 20 April 2006, doi:10.1042/BJ20051962

The Pharmacogenomics Journal (2006) 6, 388–396

www.nature.com/tpj

ORIGINAL ARTICLE

Reference profiling of the genomic response induced by an antimicrotubule agent, TZT-1027 (Soblidotin), *in vitro*

T Shimoyama[1,2], T Hamano[1], T Natsume[1], F Koizumi[1], K Kiura[2], M Tanimoto[2] and K Nishio[1,3]

[1]*Shien-Lab and Medical Oncology, National Cancer Center Hospital, Chuo-ku, Tokyo, Japan;* [2]*Department of Medicine II, Okayama University Medical School, Shikata-cho, Okayama, Japan and* [3]*Pharmacology Division, National Cancer Center Research Institution, Chuo-ku, Tokyo, Japan*

Correspondence:
Dr K Nishio, Shien-Lab, National Cancer Center Hospital, 5-1-1 Tsukiji, Chuo-ku, Tokyo 104-0045, Japan.
E-mail: knishio@gan2.res.ncc.go.jp

Received 24 October 2005; revised 20 January 2006; accepted 16 February 2006; published online 21 March 2006

TZT-1027 is an antimicrotubule agent targeting beta-tubulin that is undergoing clinical development. The genomic response of cancer cells to TZT-1027 was profiled to evaluate its biochemical activity. A lung cancer cell line, PC-14, was exposed to antimicrotubule agents including dolastatins, *Vinca* alkaloids and taxanes at an equivalent toxicity level. Alterations in the TZT-1027-induced gene expression of ~600 genes were then examined using microarray technology and the resulting gene profiles were compared with those for cells exposed to the other antimicrotubule agents. A principle component analysis using the whole gene set demonstrated that TZT-1027 produced similar gene profiles to those produced by dolastatin 10, but that these gene profiles differed from those produced by other agents. The agents were classified according to their induced genomic response in a molecular structure-dependent manner. Genes whose expression profiles differed according to drug class included intermediate filaments, extracellular matrix protein and Rho regulatory genes that may be involved in cytoskeletal and angiogenesis processes that are regulated by microtubule dynamics. TZT-1027 produces a unique genomic response profile distinct from that of *Vinca* alkaloids and taxanes, suggesting that this agent has a different mechanism of action. The selected genes may act as pharmacodynamic biomarkers allowing the unique mode of action of TZT-1027 to be discriminated from those of other antimicrotubule agents.
The Pharmacogenomics Journal (2006) **6**, 388–396. doi:10.1038/sj.tpj.6500386; published online 21 March 2006

Keywords: TZT-1027; dolastatin 10; cDNA microarray; taxanes; *Vinca* alkaloids; antimicrotubule agent

Introduction

Dolastatin 10 (D10) is small peptide inhibiting microtubule assembly and tubulin polymerization that was isolated in 1987 from an Indian Ocean mollusc, the sea hare (*Dolabella auricularia*).[1] Although D10 displayed significant antitumor activity in preclinical models and demonstrated good tolerability in clinical settings, recent phase II clinical trials suggested that D10, as a single agent, lacked significant activity.[2–5] TZT-1027 is a synthesized derivative of D10 with superior preclinical activity.[6] TZT-1027 showed notable antitumor activity against a broad range of human malignancies *in vivo*, including those resistant to conventional chemotherapeutic agents.[7] Superior antivascular activity resulting in the collapse

of the tumor vasculature was demonstrated, compared with the activities of taxanes and *Vinca* alkaloids.[8–10] The first clinical phase I study of TZT-1027 was initiated in 1994, and another four studies have since been completed; a phase II study is currently ongoing.[11–13] The major toxicity was hematological, in the form of neutropenia and leukopenia. Reversible peripheral neurotoxic syndrome, alopecia, fatigue and anorexia were the principal nonhematological toxicities.

TZT-1027 is a mitotic spindle poison that interacts with tubulin at the *Vinca* alkaloids binding site,[14] but the spectra of antitumor activity of TZT-1027 and the *Vinca* alkaloids are different *in vivo*.[7,10,15] TZT-1027 also showed potent antitumor activity against a vincristine-resistant cell line.[7] A recent investigation of the mode of action reported that TZT-1027-induced apoptosis and cell arrest in the G_2/M phase that was independent of caspase-3 or bcl-2.[16] According to *in vitro* studies performed with tumor tissue obtained from patients with lung and renal cell cancers, the activity of TZT-1027 is influenced less by the p53 mutation status than by DNA-damaging agents.[17] Despite these investigations, the mode of action and therapeutic class of TZT-1027 as an antimicrotubule agent remains unclear. To characterize the mode of action of this compound, microarray-based transcriptional profiles have been performed.[18,19]

Cell-based high-throughput screening technologies provide information about cellular pathways that control drug sensitivity.[20,21] Drug-to-drug comparative approaches using microarray analyses are useful for identifying drug targets; the cellular effects caused by a novel drug of incompletely characterized specificity can be matched to 'reference profiles' of the cellular effects elicited by the specific inhibition of candidate analog-sensitive drugs.[22,23] Thus, it has been proposed that phenotypic information generated by drug-induced alterations in gene expression can be matched to discrete interactions between the compound and the relevant protein targets. Using the drug-to-drug comparative approach of the microarray analysis, we obtained reference profiles of genomic expression data from cellular responses in a lung cancer cell line to antimicrotubule drugs, including five conventional agents and the mother compound D10. In the present study, we aimed to characterize TZT-1027 using these reference profiles.

Results

Growth inhibition

The growth inhibitory effect of TZT-1027 and the other six antimicrotubule agents was determined using an MTT assay. The PC-14 cell line was exposed to each drug for 72 h. The 50% growth inhibitory concentrations (IC_{50} values) were as follows: TZT-1027, 0.02 nM; D10, 0.1 nM; VDS, 4 nM; VBL, 2 nM; VCR, 7 nM; TXL, 3 nM and TXT, 3 nM. Based on these results, TZT-1027 was over a hundred times more cytotoxic than the other taxanes and *Vinca* alkaloids.

Microarray data mining

The expression intensity of the array was normalized using a global normalization method. The change in gene expression was calculated as the intensity ratio between treated and untreated samples. The complete cDNA microarray data can be found in the Supplementary Tables. This supporting information contains the raw data, normalized data and a summary of the selected genes.

Common genes regulated by all antimicrotubule agents

Of the 588 genes that were surveyed in the microarray analysis, 118 genes were upregulated by all seven antimicrotubules

Table 1 Gene ontology analysis of biological process of antimicrotubule agents

Upregulated		*Downregulated*	
Gene category	P	*Gene category*	P
G2/M transition of mitotic cell cycle	<0.0001	Cell–cell signaling	<0.0001
Cytokinesis	<0.0001	Morphogenesis	<0.0001
Regulation of cell cycle	0.0002	Organogenesis	0.0001
Obsolete biological process	0.0003	Development	0.0001
G1/S transition of mitotic cell cycle	0.0004	Cell communication	0.0001
Mitotic cell cycle	0.0008	Positive regulation of cell proliferation	0.0042
Apoptosis	0.0009	Growth	0.0074
Cell cycle	0.0010	Immune response	0.0098
Programmed cell death	0.0012	Defense response	0.0098
Cell death	0.0012		
Death	0.0012		
Regulation of CDK activity	0.0012		
Positive regulation of programmed cell death	0.0077		
Positive regulation of apoptosis	0.0077		
Induction of apoptosis	0.0077		
Regulation of programmed cell death	0.0077		
Induction of programmed cell death	0.0077		

agents. A functional analysis of these genes was performed using EASE, and the results are listed in Table 1. The results showed that genes associated with cell-cycle regulation, mitosis or apoptosis were significantly upregulated by the antimicrotubules agents. Among the downregulated genes, 141 genes that were associated with cell communication and morphogenesis were selected. These results suggested that transcription regulation by antimicrotubule agents results in the biological inhibition of microtubule dynamics.

Drug characterization using molecular reference profiles

Focusing on the 'reference profiles' of the drug-induced genomic response, we compared the profiles of TZT-1027 with those of five conventional antimicrotubule agents and the mother compound, D10.

A principle component representation of the whole gene set in three-dimensional space clearly showed the relationship between TZT-1027 and the other six reference profiles (Figure 1). All the drugs were separated according to each drug class in this profile. In comparison with these reference profiles, TZT-1027's profile was similar to that of D10 but different from those of the taxanes and *Vinca* alkaloids.

To investigate the differences in genomic response between the drug classes, we selected discriminatory genes that were regulated differently between the drug classes, compared with the complete gene set. Table 2 shows the genes whose expression profiles differed after exposure to dolastatins (TZT-1027 and D10) and the other antimicrotubule agents. The most discriminatory gene in this gene set was the drug-resistant gene, *GSTO1*. Using this gene set, the classes of antimicrotubule agents could be clearly separated (Figure 2a). Discriminatory gene sets for the taxanes and *Vinca* alkaloids were obtained in a similar manner (Tables 3 and 4). The profiles of the discriminatory gene sets for the taxanes and *Vinca* alkaloids are shown in Figure 2b and c.

To further characterize TZT-1027, the genes that were regulated differently after exposure to TZT-1027 and D10 were investigated. Six genes that were regulated differently by a factor of more than one in a log ratio after exposure to each agent were selected (Table 5). Four cytoskeletal genes were included in this group. A three-dimensional representation using these six genes demonstrated that the profiles

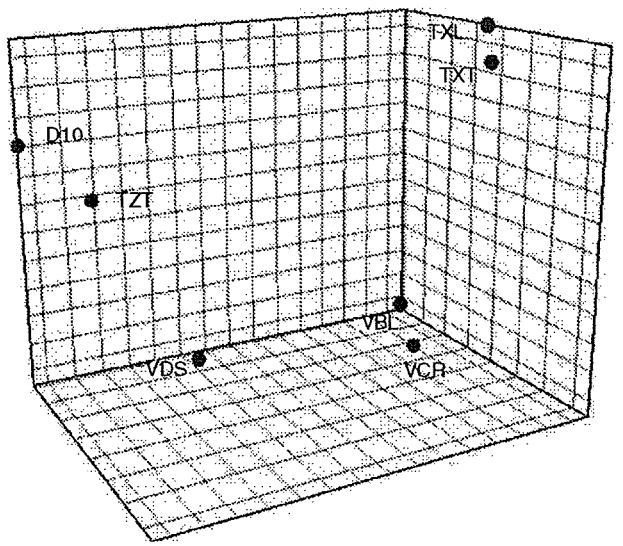

Figure 1 Three-dimensional representation of antimicrotubule agents according to a principle component analysis of the gene expression data for 588 genes. In this analysis, samples with similar expression profiles lie closer to each other than those with dissimilar profiles. The graph shows a robust class separation into three major categories: dolastatins, *Vinca* alkaloids and taxanes. TZT, TZT-1027; dolastatin 10, D10; VDS, vindesine; VCR, vincristine; VBL, vinblastine; TXL, paclitaxel; TXT, docetaxel.

Table 2 Discriminatory genes of dolastatins (D 10 and TZT-1027)

GB	*Symbol*	*Description*	*Log ratio*			
			D10	*TZT*	*VA*	*TX*
Upregulated genes						
U90313	GSTO1	Glutathione-*S*-transferase homolog	0.905	0.189	−0.818	−0.706
Z30183	TIMP3	Tissue inhibitor of metalloproteinase 3	0.703	0.481	−0.343	−0.859
U46461	DVL	Disheveled, dsh homolog 1	0.206	0.396	−0.542	−0.444
J00124	KRT1	50 kDa type I epidermal keratin	0.190	0.278	−0.643	−0.219
M57765	IL11	Interleukin 11	0.124	0.454	−0.342	−0.493
M74088	APC	Adenomatosis polyposis coli	0.040	0.069	−0.224	−0.582
Downregulated genes						
U02570	RhoGAP1	Rho-related small GTPase protein activator	−0.048	−0.076	0.433	0.248
J04177	COL11A1	Collagen, type XI, alpha 1	−0.048	−0.290	0.388	0.074
X72925	DSC1	Desmocollin-1	−0.117	−0.051	0.346	0.388
U35835	DNA-PK	DNA-dependent protein kinase	−0.215	−0.241	0.596	0.648
M65290	IL12B	Interleukin 12 beta	−0.322	−0.134	0.351	1.070

Abbreviations: GB, genebank accession number; D10, dolastatin 10; TZT, TZT-1027; VA, average of *Vinca* alkaloids including vincristine, vindesine, vinblastine; TX, average of taxanes including paclitaxel and docetaxel.

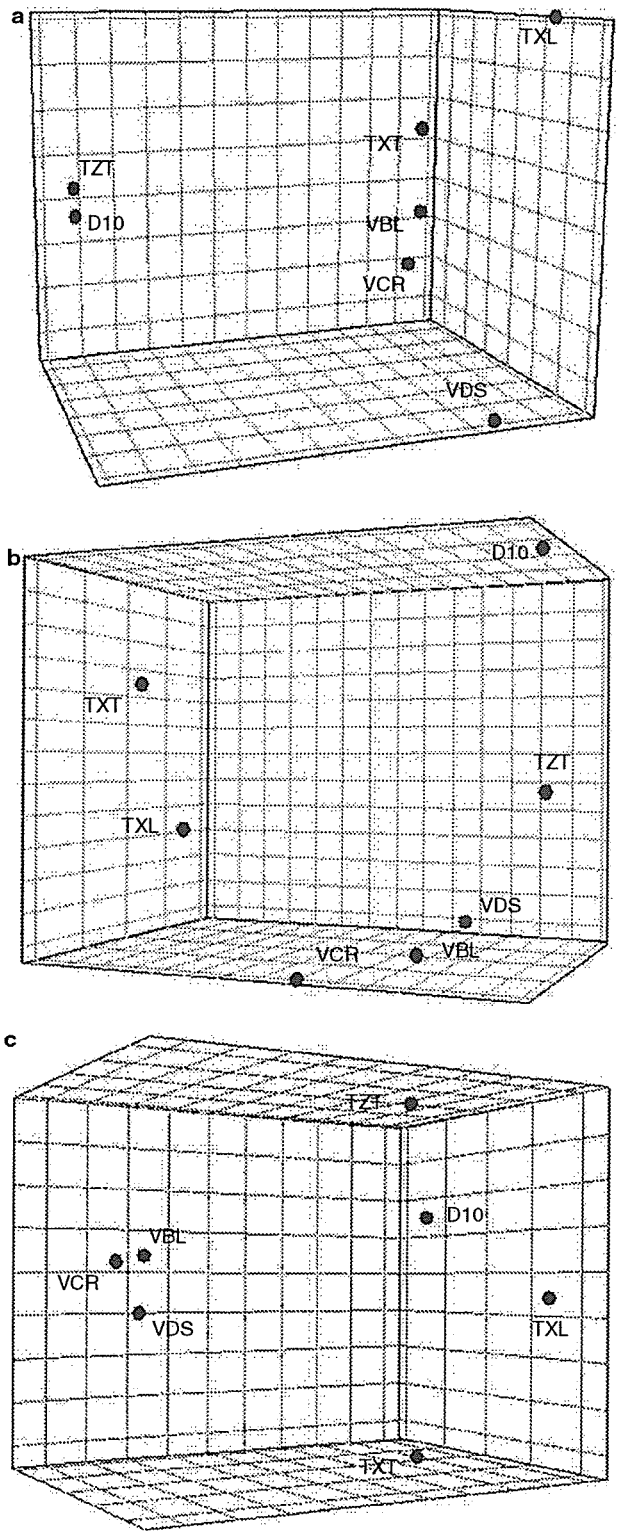

of the taxanes and *Vinca* alkaloids differed from those of TZT-1027 and D10 (Figure 3).

Validation of discriminatory genes by RT-PCR

The identified discriminatory genes GSTO1 and TIMP3 were validated using real-time RT-PCR (Figure 4). To investigate whether the genomic responses of these genes depended on the cytotoxicity levels, the RT-PCR experiment was performed at different cytotoxicity levels (IC_{90} and IC_{10}) of TZT-1027. The results are summarized in Figure 5. These findings suggested that the selected genomic responses might not depend on the cytotoxicity levels, whereas the genomic response of GSTO1 demonstrated a dose dependency.

Discussion

In the present study, we characterized the novel antimicrotubule agent TZT-1027 using a microarray analysis. Dolastatins belong to a class of microtubule-destabilizing agents, but this classification is not sufficient for clinical use. Despite similarities in their mechanism of action and structure, antimicrotubule agents differ in their antitumor and toxicologic profiles.[24] It now seems that the most important action of antimicrotubule agents is not the regulation of microtubule-polymer mass (polymerization and depolymerization), but the suppression of spindle-microtubule dynamics.[25] Furthermore, many of the drugs act not only on microtubules, but also on soluble tubulin, and the location of the specific binding site in tubulin and microtubules greatly affects the response of the microtubule system to the drug.[25] Therefore, to characterize the novel antimicrotubule agent TZT-1027, we analyzed drug-induced changes in gene expression using the microarray technique and compared the molecular profiles with those induced by the mother compound, D10, and other well-known antimicrotubule agents, such as *Vinca* alkaloids and taxanes.

For the profiles, we evaluated the IC_{50} value of each drug using a growth inhibitory assay. We aimed to categorize the drugs based on their mechanisms of action; therefore, the changes in gene expression were, of necessity, induced at the same cytotoxicity level. The resulting expression profiles were obtained using a microarray containing ~600 key genes applicable to antimicrotubule drug research, including genes involved with microtubule dynamics, cell-cycle regulation, angiogenesis and the extracellular matrix as well as cell adhesion receptors, oncogenes and tumor-suppressor genes. We focused on changes in gene expression because gene regulation should be correlated with the protein status modulated by the drugs.

Figure 2 Spatial class separation of antimicrotubule agents using specific discriminatory genes. The axes represent the first three linear discriminants of the expression levels of (a) 11 dolastatin-discriminatory genes from Table 2, (b) 9 taxane-discriminatory genes from Table 3 and (c) 5 *Vinca* alkaloid-discriminatory genes from Table 4. TZT, TZT-1027; dolastatin 10, D10; VDS, vindesine; VCR, vincristine; VBL, vinblastine; TXL, paclitaxel; TXT, docetaxel.

Table 3 Discriminatory genes of taxanes (paclitaxel, docetaxel)

GB	*Symbol*	*Description*	*Log ratio*			
			TX	*VA*	*D10*	*TZT*
Upregulated genes						
X02492	G1P3	Interferon-induced protein 6–16 precursor	1.122	−0.397	−1.150	−0.902
Y10256	NIK	Serine/threonine protein kinase	0.637	−0.951	−0.595	−0.287
U72661	NINJ1	Ninjurin 1	0.481	−0.154	−1.015	−0.448
M65199	ET2	Endothelin 2	0.444	−0.488	−2.185	−1.507
X54936	PlGF	Placenta growth factor	0.345	−0.235	−0.677	−0.602
X01992	IFN-gamma	Interferon, gamma	0.251	−0.929	−1.005	−1.583
Downregulated genes						
AF010309	PIG3	Tumor protein p53 inducible protein 3	−0.036	0.366	0.957	0.652
M76125	UFO	Tyrosine-protein kinase receptor UFO precursor	−0.132	0.201	0.020	0.329
U39657	MKK6	Mitogen-activated protein kinase 6	−0.204	0.554	0.740	0.368

Abbreviations: GB, genebank accession number; TX, average of taxanes including paclitaxel and docetaxel; VA, average of *Vinca* alkaloids including vincristine, vindesine, vinblastine; D10, dolastatin 10; TZT, TZT-1027.

Table 4 Discriminatory genes of *Vinca* alkaloids (vindesine, vincristine, vinblastine)

GB	*Symbol*	*Description*	*Log ratio*			
			VA	*TX*	*D10*	*TZT*
Upregulated genes						
X14787	TSP1	Thrombospondin 1	0.319	−0.230	−0.106	−0.019
X07820	MMP10	Matrix metalloproteinase 10	0.273	−0.272	−0.297	−0.417
Downregulated genes						
D78367	KRT12	Keratin 12	−0.124	0.262	0.250	0.598
X03212	KRT7	Keratin 7	−0.168	0.412	0.004	0.290
X56134	VIM	Vimentin	−1.072	0.583	0.927	1.344

Abbreviations: GB, genebank accession number; VA, average of *Vinca* alkaloids including vincristine, vindesine, vinblastine; TX, average of taxanes including paclitaxel and docetaxel; D10, dolastatin 10; TZT, TZT-1027.

Table 5 Discriminatory genes between TZT-1027 and dolastatin 10

GB	*Symbol*	*Description*	*Log ratio*						
			TZT	*D10*	*VDS*	*VBL*	*VCR*	*TXL*	*TXT*
U59167	DESM	Desmin	1.74	−0.49	−0.28	0.06	−0.71	0.44	0.43
U34819	MAPK10	Mitogen-activated protein kinase 10	0.83	−0.69	−0.52	0.98	0.57	1.33	0.93
X14420	COL3A1	Collagen, type III, alpha 1	0.52	−0.92	0.56	−0.79	−0.38	−0.67	−0.66
X05610	COL4A2	Collagen, type IV, alpha 2	0.71	−0.53	0.82	0.32	0.10	−0.06	0.33
X16468	COL2A1	Collagen, type II, alpha 1	1.08	−0.01	0.99	−0.08	0.56	0.36	−0.07
U33635	PTK7	Tyrosine-protein kinase-like 7	0.62	−0.45	0.04	0.56	0.68	0.15	0.05

Abbreviations: GB, genebank accession number; TZT, TZT-1027; D10, dolastatin 10; VDS, vindesine; VBL, vinblastine; VCR, vincristine; TXL, paclitaxel; TXT, docetaxel.

Of the 588 genes that were surveyed, about half of all the genes were regulated similarly by the seven drugs. The probability of these similar expression profiles occurring by chance is almost zero ($P<1\times10^{-100}$). Furthermore, the functions of the clustered genes were associated with microtubule dynamics. The 118 genes that were upregulated were significantly associated with cell-cycle regulation, mitosis or apoptosis, whereas the 141 genes that were

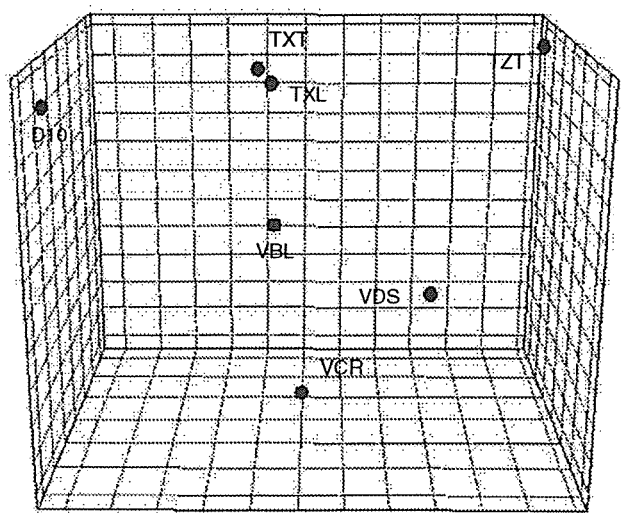

Figure 3 Spatial class separation of antimicrotubule agents using six genes from Table 5 that discriminated between TZT-1027 and dolastatin 10. TZT and D10 were distant from all the other antimicrotubule agents. TZT, TZT-1027; dolastatin 10, D10; VDS, vindesine; VCR, vincristine; VBL, vinblastine; TXL, paclitaxel; TXT, docetaxel.

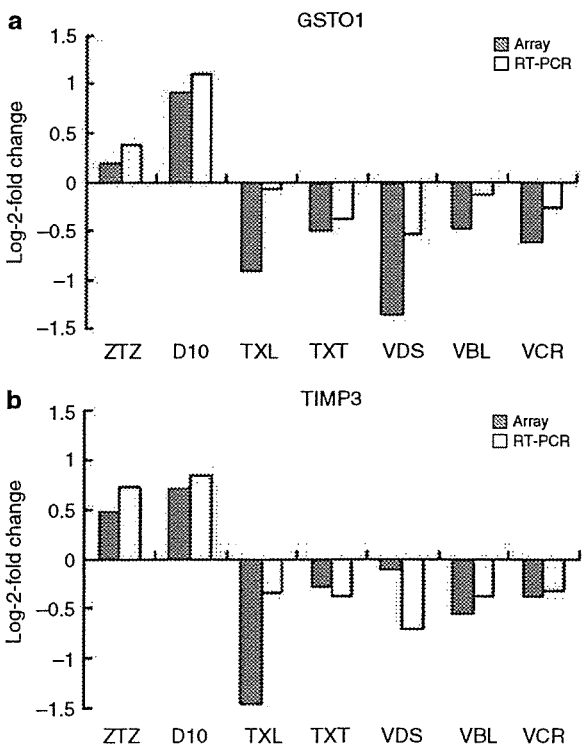

Figure 4 Gene expression of GSTO1 and TIMP3 in PC-14 cells treated with antimicrotubule agents. Validation of mRNA expression levels in PC-14 cells after 6 h of treatment with TZT-1027 (TZT), dolastatin 10 (D10), paclitaxel (TXL), docetaxel (TXT), vindesine (VDS), vinblastine (VBL) or vincristine (VCR). Relative mRNA amounts were normalized with respect to expression levels in untreated PC-14 cells (Log-2-fold change = 0).

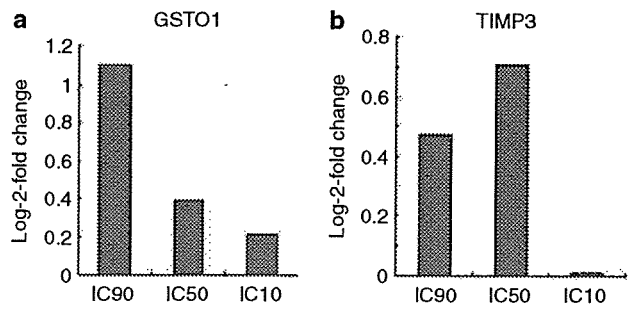

Figure 5 (a) Gene expression of GSTO1 in PC-14 cells treated with TZT-1027 at IC_{90}, IC_{50} or IC_{10}. (b) Gene expression of TIMP3 in PC-14 cells treated with TZT-1027 at IC_{90}, IC_{50} or IC_{10}. Validation of mRNA expression levels in PC-14 cells after 6 h of treatment with TZT-1027 (TZT) at IC_{90} (0.1 nM) or IC_{10} (0.005 nM).

downregulated were associated with cell communication and morphogenesis. Therefore, we concluded that the genomic response profiles represented the drug activities in PC-14 cells and investigated the discriminatory genes within each drug class to enable their further characterization.

By comparing the resulting gene profiles, each drug was categorized according to its drug class based on its effects on microtubule modulation (Figure 1). This finding suggested that genomic response was mostly affected by the drug-binding site on the microtubules. TXT shares the same tubulin-binding site as TXL, and this site is distinct from the *Vinca* alkaloids binding site.[25] Although TXL has a 1.9-fold higher affinity for the binding site and polymerizes tubulin at 2.1-fold lower concentrations than TXL,[26] TXL and TXT induced similar gene expression profiles, compared with those induced by the other antimicrotubule drugs. Among the three *Vinca* alkaloids (VBL, VDS and VCR), the expression profile of VDS differed from those of the other two (Figure 6). Natsume *et al.*[14] reported that all three *Vinca* alkaloids inhibited the polymerization of microtubules at a similar affinity. VBL and VCR are structurally very similar, whereas the structure of VDS differs from those of the other two.[27] This structural difference may be responsible for the different genomic responses. *Vinca* alkaloids and dolastatins are known to bind at so-called *Vinca*-binding domains in tubulin.[25] They share the same binding site and have similar affinities,[14,28] whereas additional binding sites have either high affinities (Kd: 1–2 μmol) or low affinities (Kd: 0.25–3 μmol).[24] Previous studies have also reported that dolastatins can also bind at different sites from those used by *Vinca* alkaloids[14,29] These additional binding sites might be responsible for the differences in genomic response induced by the dolastatins and *Vinca* alkaloids.

Interestingly, of the 31 discriminatory genes that were selected, six of them were intermediate filament (IF) genes like desmin, vimentin, desmocollin and keratin (Tables 2, 4, 5). In addition, four collagen genes and one Rho-regulator gene were also selected. These genes are all associated with cytoskeletal regulation by the Rho signaling pathway via

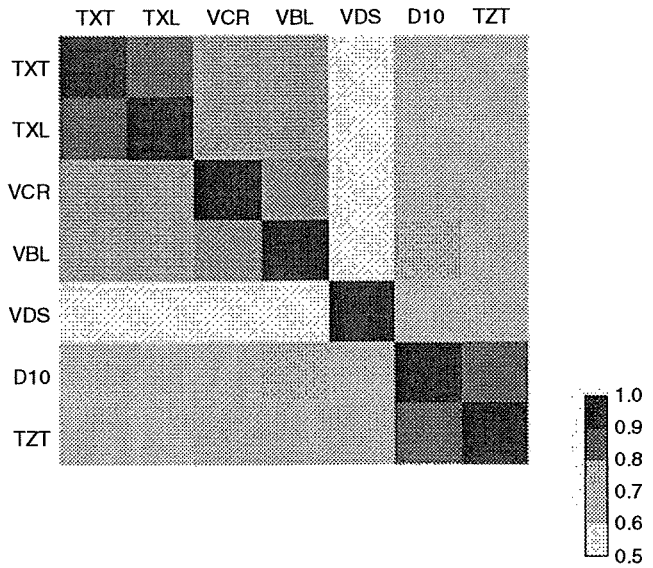

Figure 6 Heat map of correlations between drug profiles. Gene expression profiles containing data for 588 genes were compared after exposure to each drug to derive a matrix of Pearson correlation coefficients indicating the degree of overall similarity between any two drugs. A high-positive correlation is shown in red, and a low-positive correlation is shown in white. In this graph, TZT and D10 had the most similar expression profiles. TZT, TZT-1027; dolastatin 10, D10; VDS, vindesine; VCR, vincristine; VBL, vinblastine; TXL, paclitaxel; TXT, docetaxel.

microtubule dynamics.[30] Rho proteins also modulate the extracellular matrix either by regulating the levels of MMPs (matrix metalloproteinase) or their antagonists, TIMPs (tissue inhibitor of metalloproteinase).[31] These results suggested that the difference in the tubulin-drug binding site might regulate the difference in the signal transduction.

Of the genes that discriminated between dolastatins and the other drug class, the most significant genes were GSTO1 and TIMP3. GSTO1 (glutathione transferase omega 1) is a member of the glutathione *S*-transferase (GST) family of phase II enzymes that catalyze glutathione-dependent detoxification.[32] The role of GST has been evaluated in drug resistance. Schisselbauer *et al.* [33]reported that an elevated GST level in tumors was detected after the development of clinical drug resistance. Ban *et al.*[34] reported that adriamycin, cisplatin and etoposide increased tumor sensitivity by inhibiting GST expression in a colon cancer cell line, but TXL and VCR did not alter sensitivity. TIMP3 is a protein that binds to the extracellular matrix[35] and belongs to a family of endogenous MMP inhibitors. Members of the MMP family play important roles in angiogenesis.[36] Therefore, TIMP3 is regarded as a potent inhibitor of angiogenesis and tumor growth.[37] Qi *et al.*[38] reported that TIMP3 blocks the binding of VEGF (vascular endothelial growth factor) to the VEGF receptor-2, inhibiting downstream signaling and angiogenesis. TZT-1027 showed antitumor activity *in vivo* against a hypervascular advanced-stage tumor from a VEGF-transfectant lung cancer cell line, whereas VCR and TXT did not.[10] The upregulation of TIMP3 by TZT-1027 is one possible mechanism for the superior antivascular activity of this drug, compared to that of taxanes and *Vinca* alkaloids.

To analyze whether similar genomic responses occurred in lung cancer cell lines other than PC-14, RT-PCR for GSTO1 and TIMP3 was performed in another lung cancer cell line, SBC-3, treated with TZT-1027 at IC_{50}. GSTO1 and TIMP3 were downregulated in SBC-3 cells treated with dolastatins and upregulated in the cells treated with the other antimicrotubule agents, opposite to the profile seen for PC-14 cells (data not shown). This result suggested that these genes may have different genomic responses in other lung cancer cells.

This was a 'proof-of-principle study'. We demonstrated the various cellular responses to antimicrotubule agents at a gene expression level, even though the agents targeted the same molecules. We believe that this approach to characterizing drugs *in vitro* may be useful in clinical settings in that surrogate tissue, like peripheral blood mononuclear cells, can be used. The present findings obtained using our microarray analysis could greatly help us to understand the mode of action of TZT-1027 and other antimicrotubule agents. This capacity to identify therapeutic efficacy on the basis of gene expression signatures *in vitro* may be useful for drug discovery and drug target validation.

Materials and methods

Cell lines and cultures

A human non-small-cell-lung cancer cell line, PC-14, was provided by Professor Y Hayata, Tokyo Medical College. PC-14 was grown in RPMI-1640 medium (Nikken BioMedical Laboratory, Kyoto, Japan) supplemented with 10% fetal bovine serum, penicillin G and 100 μg/ml streptomycin solution and was maintained in a humidified 5% CO_2 atmosphere at 37°C.

Drugs and culture

TZT-1027 and D10 were provided by Teikoku Hormone Mfg. Co. Ltd (Kawasaki, Japan) and were dissolved in and diluted with 0.05 M lactate buffer (pH 4.5). Vindesine (VDS), vincristine (VCR), vinblastine (VBL), docetaxel (TXT) and paclitaxel (TXL) were obtained from Shionogi Co. (Osaka, Japan), Shionogi Pharmaceutical Co. (Osaka, Japan), Kyorin Pharmaceutical Co. Ltd (Tokyo, Japan), Chugai-Seiyaku Co, Ltd (Tokyo, Japan) and Bristol-Myers Japan (Tokyo, Japan), respectively. RPMI 1640 medium (Gibe-BRL) and fetal bovine serum were purchased from Nisus (Tokyo, Japan).

MTT assay

The inhibitory effect of the drugs on the PC-14 cell line was determined using a colorimetric assay (MTT assay) according to the method of Mosmann.[39] Briefly, 10^3 cells were harvested in 96-well microtiter plates (Becton Dickinson & Co.) in a volume of 180 μl and incubated for 24 h at 37°C in humidified air containing 5% CO_2. Each drug was added to